UNIVERSITY OF CALIFORNIA,
IRVINE

Understanding the effects of the myocardial environment on the organization and cellular viability in hearts with and without pathology

DISSERTATION

submitted in partial satisfaction of the requirements
for the degree of

DOCTOR OF PHILOSOPHY

in Biomedical Engineering

by

Richard D.H. Tran

Dissertation Committee:
Associate Professor Anna Grosberg, Chair
Associate Professor Michael Zaragoza
Associate Professor Joshua Mauney

2021

TABLE OF CONTENTS

LIST OF FIGURES

Page

LIST OF TABLES

Page

ACKNOWLEDGEMENTS

I would like to thank my advisor, Dr. Anna Grosberg, for her support, mentorship, and teachings throughout my Ph.D.

I would also like to acknowledge all members of the Cardiovascular Modeling Laboratory for their collaborative talks and help they have given me during my time at UCI.

I would like to thank the colleagues from other labs in the Edwards Lifesciences Center for Advanced Cardiovascular Technology for their help during both projects.

I would like to thank our collaborators Professor Samuel Safran, Professor Eran Bouchbinder, Ohad Cohen, Dan Deviri, and Avraham Moriel for discussions related to these works.

I would also like to give a special thanks to my dissertation committee members, Dr. Michael Zaragoza and Dr. Joshua Mauney, and my advancement committee members, Dr. Wendy Liu and Dr. Timothy Downing.

This work was supported by the National Institute of Health (NIH) National Institute T32 Training Grant in Cardiovascular Applied Research and Entrepreneurship (5T32 HL116270-3), R01 HL129008 (PIs: Grosberg and Zaragoza), R03 EB028605. This work was also (partially) supported by an NSF grant, DMS1763272, and a grant from the Simons Foundation (594598).

VITA

RICHARD D.H. TRAN

Education

Ph.D. in Biomedical Engineering, University of California, Irvine, CA 2016-2021
Masters in Biomedical Engineering, University of California, Irvine, CA 2016-2020
Bachelors in Biomedical Engineering, University of California, Irvine, CA 2012-2016

Research Experience

University of California Irvine Irvine, CA
Graduate Student Researcher - Cardiovascular Modeling Laboratory 2016-2021

- Designed and performed multiple experiments using a biomechanical stretching device with self-developed protocols to examine the effects of cyclic strain on 20 different patient specific cell lines with and without *LMNA* mutations
- Differentiated induced pluripotent stem cells of patient specific cell lines into cardiomyocytes to investigate how the *LMNA* mutation affects the structure and function of cardiac tissue through the use of a Heart-on-a-Chip device
- Developed a new approach to study how cells organize in the heart through the combination of co-cultures and the application of cyclic strain
- Utilized drugs to inhibit intercellular junction formation to study the effects of cell-cell contact on cellular organization of cardiac cells in response to cyclic mechanical strain
- Lead multiple interdisciplinary collaborations to explore how different mechanical strain profiles or microfluidic stimulation could affect cells with the *LMNA* mutation

Undergraduate Research Assistant - Metabolic Imaging Biochemistry Lab 2014-2016

- Practiced experimental design, planning, and execution
- Maintained and cultured multiple breast cancer cell lines in both 2D and 3D cultures to examine development and differences in the metabolism
- Examined and analyzed cellular chemical levels of breast cancer cells to quantify metabolism rate by using MATLAB and ImageJ as post-processing on fluorescence imaged samples

Prolacta Bioscience City of Industry, CA
Research and Development Intern Jun-Sep 2015

- Conducted multiple experiments independently under the mentorship of the Senior R&D Director
- Participated in the development and formation of a new milk formula for premature infants in neonatal care

- Performed product yield experiments in a clean room with industrial grade equipment
- Collaborated and coordinated with multiple departments to develop and test a new formula in line with customer needs

AWARDS

Watson Land Company Scholarship 2012-2016
Center for Complex Biology Systems (CCBS) Opportunity Award 2016
Center for Multiscale Cell Fate Research (CMCF) Interdisciplinary Opportunity Award 2020
Cardiovascular Applied Research and Entrepreneurship (CARE) Fellowship 2019-2021

PUBLICATIONS

R. D.H. Tran, M. Siemens, C. H. H. Nguyen, A. R. Ochs, M. V. Zaragoza, and A. Grosberg, "The Effect of Cyclic Strain on Human Fibroblasts with Lamin A/C Mutations and Its Relation to Heart Disease," *J Biomech Eng*, 2019.

R. D.H. Tran*, T. Morris*, D. Gonzalez, A. Hetta, and A. Grosberg, "Quantitative Evaluation of Cardiac Cell Interactions and Responses to Cyclic Strain." Submited 2021.

J. Hou, H. J. Wright, **R. Tran**, N. Chan, O. V. Razorenova, E. O. Potma, and B. J. Tromberg, "Correlating two-photon excited fluorescence imaging of breast cancer cellular redox state with seahorse flux analysis of normalized cellular oxygen consumption," *Journal of Biomedical Optics*, vol. 21, 2016.

T. Morris, **R. D.H. Tran**, and A. Grosberg, "A Comprehensive Review of Computational and Image Analysis Techniques for Quantitative Evaluation of Striated Muscle Tissue Architecture." Biophysics Review. Submitted 2021.

TALKS/POSTERS PRESENTED

19th Annual UC Systemwide Bioengineering Symposium 2018
Poster: "The effect of heart mechanics on cells with the Lamin A/C mutation and its relation to heart disease"
Authors: Richard Tran, Alex Ochs, Linda McCarthy, Cecilia Nguyen, Mark Siemens, Michael Zaragoza, Anna Grosberg

NanoEngineering for Medicine and Biology (NEMB) – ASME 2018
Talk: "The effect of heart mechanics on the nuclear properties of cells with the Lamin A/C mutation and its relation to heart disease"
Authors: Richard Tran, Alex Ochs, Linda McCarthy, Cecilia Nguyen, Mark Siemens, Michael Zaragoza, Anna Grosberg

CMCF Early Career Researcher Symposium 2021
Talk: Cardiac Cells Under Mechanical Stimulation: A Combined Mathematical, Computational and Experimental Approach
Authors: Richard Tran, Tessa Morris, Avraham Moriel, Eran Bouchbinder, Samuel Safran, Anna Grosberg

ABSTRACT OF THE DISSERTATION

Understanding the effects of the myocardial environment on the organization and cellular viability in hearts with and without pathology

By

Richard D.H. Tran

Doctor of Philosophy in Biomedical Engineering

University of California, Irvine, 2021

Associate Professor Anna Grosberg, Chair

The heart is a vital organ that pumps blood throughout the body by constantly, cyclically contracting. Unfortunately, the heart can be vulnerable a wide range of diseases and injuries. In order to truly predict, prevent, or treat diseases in the heart, the myocardial environment and how it affects myocardial repair and pathways that lead to cardiac diseases should be thoroughly investigated. However, the complex structure, genetic and environmental factors, and inaccessibility *in vivo* make it difficult to fully elucidate the mechanisms behind cardiac remodeling and repair. Thus, to truly study the heart, it is necessary to develop *in vitro* models that can closely recapitulate the myocardial environment to methodically investigate the isolated mechanisms.

The heart has a unique dynamic mechanical environment that is closely linked to its highly organized structure and specialized cells. This mechanical environment is contributed to the unique composition of cell types and the resultant structure of the tissue. Interestingly, in some heart diseases, this organization and cellular composition is disrupted, which results in loss of efficient

heart function. Additionally, as the heart contracts, all the resident cells are also exposed to unique mechanical strains which can affect their function and organization. To create an accurate *in vitro* model of the myocardium, the mechanical strains and cellular composition of the heart should be considered. However, it is not fully known what cells contribute to the highly organized structure of the heart and how the cells are affected by mechanical strain.

To address these problems, we recapitulated *in vitro* both the dynamic mechanical environment of the heart and its cellular composition to demonstrate how these factors can affect the organization, morphology, and viability of cardiac cells. In order to understand how cardiac cells organize in healthy or pathological heart tissue, we applied cyclic strain to co-cultures of the two most dominant cell types within the heart, cardiomyocytes and fibroblasts. Our results illustrates that cardiomyocytes and fibroblasts do influence the organization of one another. Additionally, to recreate *in vitro* the organization or lack thereof observed in healthy and fibrotic heart tissue respectively, we examined tissue exposed to cyclic strain with various densities of cardiomyocytes and fibroblasts. Furthermore, when we investigated if intercellular junctions could affect organization, there were no changes in the overall orientation of the two cell types when junction formation was inhibited with drugs. Thus, either these intercellular junctions are more important in the myocardium or they play a secondary role in organization relative to the amount of cells present.

Additionally, in this dissertation we examined how mechanics mimicking the myocardial environment affects cells with and without a *LMNA* mutation. To investigate this, we used patient specific cells and subjected them to cyclic strains before quantifying the cell viability/proliferation, cytoskeleton and extracellular matrix organization, proportion of dysmorphic nuclei, and nuclear shape. Though our results indicated that cyclic strain alone was insufficient to cause any significant

differences that could explain the mechanisms that lead to heart diseases in these patients with *LMNA* mutations, we were able to observe these differences in cells with a severe type of the *LMNA* mutation.

Overall, our results highlight the influence that different cell types have on heart tissue organization. Additionally, we emphasize the importance of the unique mechanical environment of the heart when examining cardiac tissue organization and cells with genetic mutations. The work done in this dissertation will serve as a foundation for future models of the heart that study cardiac remodeling, repair, and diseases.

CHAPTER 1

INTRODUCTION

The heart has a unique dynamic mechanical environment that is closely linked to its highly organized structure and specialized cells. This mechanical environment is contributed to the unique composition of cell types and the resultant structure of the tissue. Within the heart, there are many different cell types that assemble together in order to generate the cyclical forces that allow the heart to pump blood. As the heart contracts, all the resident cells are also exposed to unique mechanical strains[1,2]. Since exposure to mechanical strain can affect cellular function and organization this emphasizes the importance of the mechanical environment of the heart[3–8]. Still, how the mechanisms of the myocardial environment contributes to heart injury development or disease progression is not fully understood.

One mechanism not fully understood is how the cellular composition of the heart affects cardiac remodeling and repair. Of the multitude of cells residing within the heart, the two dominant cell types are cardiomyocytes and fibroblasts[9,10]. While cardiomyocytes are the primary functional cell type, fibroblasts also play many important roles in the heart such as extracellular matrix maintenance, secreting cytokines and growth factors, and more[11–13]. In healthy heart tissue, where organization is a vital factor in determining the forces produced during contraction, both of these cells are observed to be well-organized along the direction of strain[14]. However, in post infarction and heart diseases, this organization and cellular composition is disrupted resulting in loss of efficient heart function[3–8]. There are many *in vivo* models that study cardiovascular diseases, but the complexity, genetic factors, and environmental factors make it difficult to create a perfect

experimental model[15]. In order to truly study cardiac remodeling and repair, the mechanisms responsible must be isolated and studied methodically in cardiac tissue created *in vitro*. Current *in vitro* studies involving cardiac cells use methods such as micropatterning, microgroving, or mechanical strains to guide cells to organize in a specified manner[16]. By establishing methods to organize cells in a dish, it is possible to create highly organized cardiac tissue that resemble the heart. Though there are multiple methods to organize cells, with the heart having a dynamic mechanical environment, utilizing strain as a method of promoting reorganization is particularly intriguing. Furthermore, to closely recapitulate the myocardial environment, the cellular composition should also be considered in conjunction with organization since the heart is composed of many different cell types. The combination of organization and co-cultures to create *in vitro* heart tissue could prove to be a useful tool that has not been studied yet. In creating a reliable method to capture the myocardial environment *in vitro*, it could further the understanding of how the heart responds to infarction or disease and advance tissue engineer therapeutics in the future.

In vitro models are also an important tool used to study genetic mutations that can affect the heart in patient specific cells. Though, as *in vivo* studies are inaccessible, to study the genetic mutations in these patients, it is necessary to recapitulate the myocardial environment *in vitro*. The *in vitro* models should not only consider the organization of the cells, but also the strains the cells experience as the hearts of the affect patients have altered force generation[17,18]. Furthermore, to investigate diseases in patients, there needs to be a source of cells that is easily accessible in all patient groups. By carefully utilizing *in vitro* methods and an easily accessible patient specific cell source to capture the myocardial environment, it will be possible to understand how genetic mutations lead to heart diseases in patients.

In this thesis, we present work that utilizes the dynamic mechanical environment of the heart to elucidate the development of both healthy and pathological hearts *in vitro*. In Chapter 2, we investigate how different cardiac cellular compositions and intercellular junctions effect heart tissue organization. This was accomplished by identifying specific physiological relevant densities of cardiomyocytes and fibroblasts and exposing them to cyclic stains resembling the myocardial environment and/or intercellular junction inhibitory drugs. Following, in Chapter 3, we examine how the application of similar cyclic strains can affect cells with and without the *LMNA* mutation by looking at morphological nuclear and extracellular matrix differences. Future work, Chapter 4, will outline the next steps in continuing these studies and plans to explore using cells shed in urine as an alternative and easily accessible source of cells to study heart disease in a large population. The work done in this thesis emphasizes the importance of incorporating mechanics in models involving the heart as well as creating experimental platforms that more closely recapitulates the myocardial environment biologically and mechanically.

REFERENCES

1. Matthew W. Curtis and Brenda Russell. Micromechanical regulation in cardiac myocytes and fibroblasts: Implications for tissue remodeling, 2011. ISSN 00316768.
2. John Shaw, Leighton Izu, and Ye Chen-Izu. Mechanical Analysis of Single Myocyte Contraction in a 3-D Elastic Matrix. *PLoS ONE*, 8(10), 2013. ISSN 19326203. doi: 10.1371/journal.pone.0075492.
3. Carlo Alberto Beltrami, Nicoletta Finato, Maurizio Rocco, Giorgio A. Feruglio, Cesare Puricelli, Elena Cigola, Edmund H. Sonnenblick, Giorgio Olivetti, and Piero Anversa. The cellular basis of dilated cardiomyopathy in humans. *Journal of Molecular and Cellular Cardiology*, 27(1):291–305, 1995. ISSN 00222828. doi: 10.1016/S00222828(08)80028-4.
4. Patrizia Camelliti, Gerard P. Devlin, Kenneth G. Matthews, Peter Kohl, and Colin R. Green. Spatially and temporally distinct expression of fibroblast connexins after sheep ventricular infarction. *Cardiovascular Research*, 62(2):415–425, 2004. ISSN 00086363. doi: 10.1016/j.cardiores.2004.01.027.
5. Claudio Humeres and Nikolaos G. Frangogiannis. Fibroblasts in the Infarcted, Remodeling, and Failing Heart, 2019. ISSN 2452302X.
6. Wei Chen and Nikolaos G. Frangogiannis. Fibroblasts in post-infarction inflammation and cardiac repair, 2013. ISSN 01674889.
7. Ronald B. Driesen, Fons K. Verheyen, Petra Dijkstra, Fred Thoné, Jack P. Cleutjens, Marie Helénè Lenders, Frans C.S. Ramaekers, and Marcel Borgers. Structural remodelling of cardiomyocytes in the border zone of infarcted rabbit heart. *Molecular and Cellular Biochemistry*, 302(1-2), 2007. ISSN 03008177. doi: 10.1007/s11010-007-9445-2.
8. Eeva Palojoki, Antti Saraste, Anders Eriksson, Kari Pulkki, Markku Kallajoki, Liisa Maria Voipio-Pulkki, and Ilkka Tikkanen. Cardiomyocyte apoptosis and ventricular remodeling after myocardial infarction in rats. *American Journal of Physiology - Heart and Circulatory Physiology*, 280(6 49-6), 2001. ISSN 03636135. doi: 10.1152/ajpheart.2001.280.6.h2726.
9. Meghan B Knight, Anna Grosberg, and Megan L McCain. In Vitro Tools for Quantifying Structure–Function Relationships in Cardiac Myocyte Cells and Tissues. In *Cardiac Cytoarchitecture*, pages 15–39. Springer, 2015.
10. H. W. Vliegen, A. Van Der Laarse, C. J. Cornelisse, and F. Eulderink. Myocardial changes in pressure overload-induced left ventricular hypertrophy: A study on tissue composition, polyploidization and multinucleation. *European Heart Journal*, 12(4):488–494, 1991. ISSN 0195668X. doi: 10.1093/ oxfordjournals.eurheartj.a059928.
11. C A Souders, S L K Bowers, and T A Baudino. Cardiac Fibroblast The Renaissance Cell. *Circulation Research*, 105(12):1164–1176, 2009. ISSN 0009-7330. doi: 10.1161/Circresaha.109.209809.
12. Peter Kohl and Robert G. Gourdie. Fibroblast-myocyte electrotonic coupling: Does it occur in native cardiac tissue?, 2014. ISSN 10958584.
13. Patrizia Camelliti, Thomas K. Borg, and Peter Kohl. Structural and functional characterisation of cardiac fibroblasts, 2005. ISSN 00086363.
14. Richard A. Lasher, Aric Q. Pahnke, Jeffrey M. Johnson, Frank B. Sachse, and Robert W. Hitchcock. Electrical stimulation directs engineered cardiac tissue to an age-matched

native phenotype. *Journal of Tissue Engineering*, 3(1), 2012. ISSN 20417314. doi: 10.1177/2041731412455354.

15. Daniela Fliegner, Christoph Gerdes, Jörg Meding, and Johannes Peter Stasch. Translational in vivo models for cardiovascular diseases. In *Handbook of Experimental Pharmacology*, volume 232. 2016. doi: 10.1007/164fn g2015fn g31.
16. Adrian Martinez-Rivas, Genèsis K. González-Quijano, Sergio Proa-Coronado, Childérick Séverac, and Etienne Dague. Methods of micropatterning and manipulation of cells for biomedical applications, 2017. ISSN 2072666X.
17. Jeffrey R. Moore, Leslie Leinwand, and David M. Warshaw. Understanding cardiomyopathy phenotypes based on the functional impact of mutations in the myosin motor, 2012. ISSN 00097330.
18. Theresia Kraft and Judith Montag. Altered force generation and cell-to-cell contractile imbalance in hypertrophic cardiomyopathy, 2019. ISSN 14322013.

CHAPTER 2

Quantitative Evaluation of Cardiac Cell Interactions and Responses to Cyclic Strain[1]

ABSTRACT

The heart has a dynamic mechanical environment contributed by its unique cellular composition and the resultant complex tissue structure. In pathological heart tissue, both the mechanics and cell composition can change and influence each other. As a result, the interplay between the cell phenotype and mechanical stimulation needs to be considered to understand the biophysical cell interactions and organization in healthy and diseased myocardium. In this work, we hypothesized that the overall tissue organization is controlled by varying densities of cardiomyocytes and fibroblasts in the heart. In order to test this hypothesis, we utilized a combination of mechanical strain, co-cultures of different cell types, and inhibitory drugs that block intercellular junction formation. To accomplish this, an image analysis pipeline was developed to automatically measure cell type specific organization relative to the stretch direction. The results indicated that cardiac cell type specific densities influence the overall organization of heart tissue such that it is possible to model healthy and fibrotic heart tissue *in vitro*. This study provides insight on how to mimic the dynamic mechanical environment of the heart in engineered tissue, as well as provide valuable information about the process of cardiac remodeling and repair in diseased hearts.

[1] Tran, Richard D.H.*, Morris, Tessa Altari* et al. (2021) Submitted to *Cells*

INTRODUCTION

The two dominant cell types in the myocardium are cardiomyocytes and cardiac fibroblasts; cardiomyocytes generate contractile force[1–3], while fibroblasts play vital roles in maintaining functions within the heart such as extracellular matrix production, cardiac remodeling, cell-cell signaling, promoting blood vessel formation, and secretion of growth factors and cytokines[4–6]. In a healthy heart, cardiomyocytes and fibroblasts are organized along the direction of contraction[7–9]. However, in the event of myocardial infarction or other cardiac diseases, there is increased migration of fibroblasts into the regions of damaged tissue as well as changes to the morphology and viability of the myocytes[10–15]. The alterations in cellular composition and structure result in disorganization and loss of efficient heart function[16–18].

Although cellular disorganization, as well as a shift in the dominant cell type as a result of injury or remodeling such as fibrosis has been observed, the mechanisms that drive the organization of cardiomyocytes and fibroblasts and how they influence each other are not fully understood. Investigating the mechanisms responsible for organization in the heart is imperative to create accurate *in vitro* models of infarcted or diseased hearts, propose new pathways for treatment, and improve tissue engineering approaches such as cardiac patches[19–21]. To elucidate these mechanisms, cardiac cellular organization has been examined using a plethora of *in vitro* approaches[22,23]. In particular, one factor that is commonly implicated as a driving force for cellular organization is the application of strain to the cells[24–28]. Though several studies have shown that cells respond and organize when exposed to static/cyclic strains/stresses, the response is not consistent for all cardiac cell types[27,29–33]. Counter to what is observed in healthy myocardium, where both cell types are present and co-oriented parallel to contraction, in isolated *in vitro* cultures that are exposed to uniaxial cyclic strain, fibroblasts orient approximately perpendicular to the

strain direction[25,30,34], while cardiomyocytes orient approximately along the direction of mechanical stimulation[35]. A full understanding of the factors that may contribute to how cells organize in healthy heart tissue is essential for a slew of applications.

An unexplored factor that may be responsible for how cells organize in the heart is the interaction between the different cell types. In highly organized cardiac tissue, cardiomyocytes and fibroblasts are indirect contact with each other. To communicate, the cardiac cells are electrically and mechanically coupled via gap and adherens junctions, both heterogeneously (i.e. cardiomyocyte-fibroblast) and homogeneously (i.e. cardiomyocyte-cardiomyocyte and fibroblast-fibroblast)[36]. The most abundant gap and adherens junctions in the heart are Connexin 40 (Cx40), Connexin 43 (Cx43), and Connexin 45 (Cx45), and N-cadherin (N-cad), respectively[1,6,26,36–40]. Interestingly, by inhibiting or blocking a subset of these junctions, studies have shown inhibited cell-cell contact, adhesion, and signaling between cells[1,26,36,39,41–44]. Therefore, observing interactions between distinct cardiac cell types in confluent co-cultures through intercellular junctions or physical contact may be necessary to understand the guiding mechanisms for cardiac tissue reorganization in its native dynamic mechanical environment.

In this work, we created a system to study if different cardiac cellular compositions and intercellular junctions have an effect on heart tissue organization. To study this, we identified specific densities that are relevant to physiological states to examine how heart tissue organizes in response to cyclic strain. In addition, we investigated certain intercellular junctions that are abundant in the heart to elucidate their role in the tissue organization. To quantify the differences in cellular organization under each experimental condition, we developed a classifier that is able to distinguish between cardiac cell types and quantified the orientational organization of the cell types separately[45]. These experiments allowed us to elucidate the interaction between multiple

cardiac cell types and several intercellular junctions to explain the organization behavior in healthy and diseased heart tissue.

RESULTS

Studying how cardiomyocytes and fibroblasts organize in response to mechanical stimulation required the ability to reliably separate them in images and measure their individual orientation. A classifier was developed to distinguish between the different cardiac cell types[45]. With the successful classification, the principal direction (director) and the spread in the distribution of the orientation vectors, orientational order parameter (OOP), was quantified. Then with the cell type specific director and the OOP, we were able to quantify the alignment and orientation of the different cell types.

In order to understand the guiding mechanisms for cardiac tissue reorganization in a dynamic mechanical environment, cardiomyocytes and fibroblasts were co-cultured at different densities (Table 2.1 & Figure 2.1A-D) in a stretcher device and were exposed to 15% cyclic uniaxial strain at 1 Hz for 48 hr. To prevent any bias, all of the data was preserved even though in some cases the seeding densities did not match the actual densities measured by the cell type actin fraction (Figure 2.1E-H). As a consequence, a few of the cultures were sparser than expected and resulted with the cells orienting to their preferential direction (i.e. Figure 2.1E-F, arrows). For confluent monocultures of cardiomyocytes, cells organized as previously observed *in vitro*[34,36], approximately parallel to the direction of stretch (Figure 2.1A, E at 40k:≈0). Similarly, fibroblasts seeded as a monoculture also organized as expected, approximately perpendicular to the direction of stretch (Figure 2.1D, G at ≈0:40k) [25,30,34,35]. However, for co-cultures, the principal direction of both cardiomyocyte and fibroblast actin relative to stretch changed depending on the dominant cell type (Figure 2.1E-H). At the 4:1, 2:1, and 1:2 cardiomyocyte to fibroblast seeding densities,

cardiomyocytes gradually transitioned from the parallel direction to a direction perpendicular with respect to stretch (Figure 2.1E 40k:10k, 30k:15k, 15k:30k respectively). The OOP of the cardiomyocyte actin was also lower at the intermediate ratios, indicating that there was high variability in the alignment of the cardiomyocytes with respect to stretch (Figure 2.1I,J between 0.2-0.8). This is particularly evident at the 2:1 and 1:2 ratios where neighboring cardiomyocytes can be oriented in different directions when examined qualitatively (Figure 2.1E 30k:15k and 15k:30k respectively). It was also observed that for cardiomyocytes and fibroblasts at the intermediate ratios, 4:1 and 2:1,where the influence exerted by the prevalent cell type was not dominant enough to dictate organization fully, the two cell types have different average direction with respect to stretch, (i.e. directors) (Figure 2.1E,G 40k:10k and 30k:15k respectively). This suggest that how the cells are orienting is part of a stochastic process where which cells adhere to the culture first can influence the spread and amount of cell-cell contact with one another. As seen in the intermediate densities with both cell types, the randomness can easily be distinguished from the highly organized edges (Figure 2.1F,H-J fractions <0.2 and >0.8).

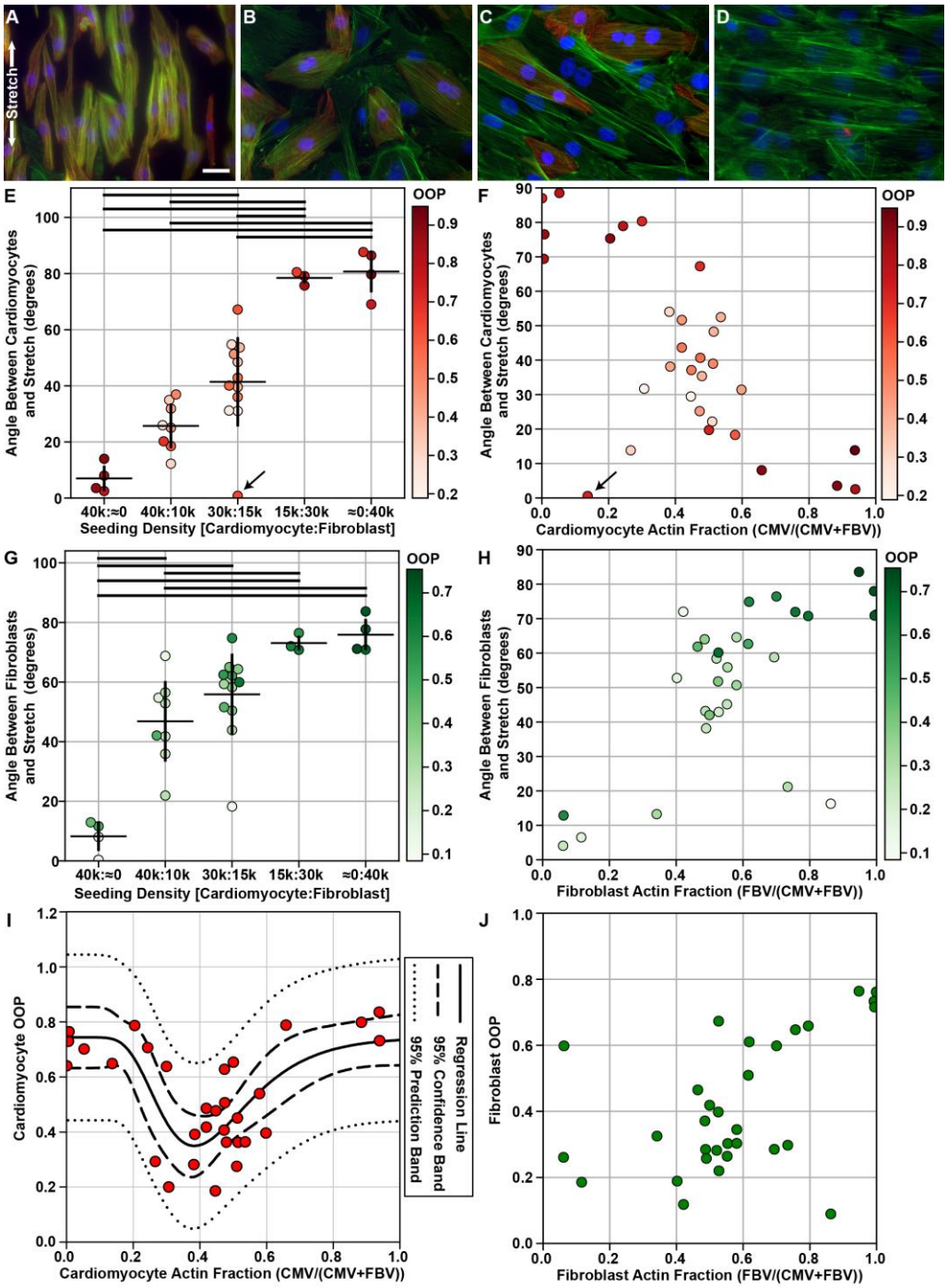

Figure 2.1 Cell type specific actin orientation with respect to the direction of applied cyclic strain for different co-culture densities. Representative images of different experimental co-culture densities (A) 40k:≈0 (B)30k:15k (C) 15k:30k (D) ≈0:40k labeled with α-actinin (red), actin (green), and DAPI (blue). (E) The average and standard deviation of the angle between the cardiomyocyte actin director and stretch director for each experimental seeding density. (F) The angle between the cardiomyocyte actin director and stretch director for the measured cell type actin fraction i.e., the total number of cardiomyocyte actin vectors divided by the total number actin

vectors. (G) The average and standard deviation of the angle between the fibroblast actin director and stretch director for each experimental seeding density. (H) The angle between the fibroblast actin director and stretch director for the measured cell type actin fraction i.e., the total number of fibroblast actin vectors divided by the total number actin vectors. (I) Cardiomyocyte OOP as a function of actin fraction; Fitted with a log normal equation ($p<0.05$); Regression line (solid), 95% confidence interval (dashed), and 95% prediction band (dotted). (J) Fibroblast OOP as a function of actin fraction. In A and B, the arrows indicate a well with sparser than expected density. In E-J, each point represents a single well, which is colored by the actin OOP for cardiomyocytes (E,F,I) or fibroblasts (G,H,J). In E and G, horizontal bars indicate groups with significantly different means ($p<0.05$). All scale bars: 25μm.

Table 1.1 Co-Culture Cell Type Ratios

CM:FB Seeding Ratio	Description	Relevance
≈0:1	Fibroblast Dominant	Recapitulate published results
1:2	Fibroblast Dominant	Intermediate; Beginning of injury/inflammation
2:1	Cardiomyocyte Dominant	Physiologically Relevant
4:1	Cardiomyocyte Dominant	Rare Fibroblast
1:≈0	Cardiomyocyte Dominant	Recapitulate published results

The fibroblast orientation was also a function of the seeding densities. At seeding densities with higher amounts of fibroblasts, 1:2 and ≈0:1, the principal direction of cardiomyocytes generally follow the fibroblast preferred orientation (close to perpendicular to stretch) and thus had a relatively high OOP (Figure 2.1G,H 15k:30k and ≈0:40k respectively). The principal direction between fibroblasts and the stretch direction gradually decreased as there were relatively more cardiomyocytes (Figure 2.1G,H). However, unlike the cardiomyocytes, the fibroblast actin OOP decreased with the relative number of fibroblasts (Figure 2.1J). From these results, for both cardiomyocytes and fibroblasts, the presence of the other cell type caused a deviation from their observed orientation in monocultures when exposed to cyclic strain.

$$y = y_0 + \frac{a}{x} exp\left[-0.5\left(\frac{ln\left(\frac{x}{x_0}\right)}{b}\right)^2\right] \quad (1)$$

Table 2.2 Log Normal Fit Details

Variable	Description or Coefficient	Significance
x	Cardiomyocyte Actin Fraction	N/A
y	Cardiomyocyte OOP	N/A
a	-0.1605	<0.0001
b	0.3504	0.0006
x_0	0.4334	<0.0001
y_0	0.7437	<0.0001
R^2		0.5554

Cardiomyocyte organization as a function of cardiomyocyte actin fraction is well described by a lognormal equation (Equation 1 & Figure 2.1I). The data is well fitted as seen with the strong p-values (Table 2.2) and the 95% confidence and prediction bands. When cardiomyocytes occupied approximately a 35% of the culture, this corresponded to an area with low organization indicated by the minimum of the regression line (Figure 2.1I). The tail ends of organization on the left and right of the fit represented areas with high organization where cardiomyocytes were guided by fibroblasts or by each other, respectively (Figure 2.1I <0.2 and >0.8). In contrast, fibroblast OOP did not have an obvious minimum and could not be fitted similarly (Figure 2.1J). From previous experiments with cardiomyocytes, it is known that fibroblasts are more dynamic and often spread into areas with no cells. As a result, fibroblasts can orient in the direction they move or spread even without guidance. In consequence, fibroblasts have more randomness to their organization, which is seen when examining fibroblast organization as a function of fibroblast actin fraction especially at densities where there is low amounts of fibroblasts (Figure 2.1J fractions <0.2). Thus, to understand organization of heart tissue, it is important to look at the OOP of cardiomyocytes and fibroblasts separately.

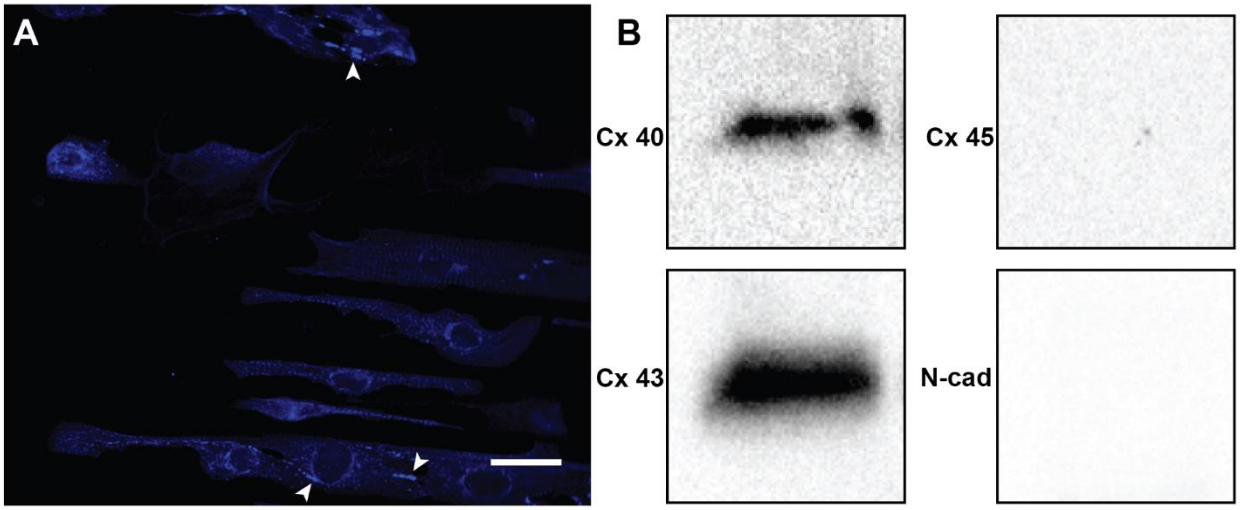

Figure 2.2 Intercellular junction presence. Cells stained for the presence of Connexin 43. (A) Example image of a sampled stained for Connexin 43; Arrows indicate areas with noticeable Connexin 43 junctions; Scale bar: 25 μm. (B) Western blot of Connexins 40, 43, and 45 and N-cadherin.

To test whether inhibiting the formation of gap and adherens junctions between cells is sufficient to impact the organizational interaction between cardiomyocytes and fibroblasts, we first confirmed their presence in our cultures (Figure 2.2A). Due to difficulty quantifying the amounts of protein in the images, western blotting was used to confirm the presence of each protein (Figure 2.2B). From the blots, only Cx40 and Cx43 were found to be present in these cells (Figure 2.2B & Figure 2.4). Even though some proteins, Cx45 and N-cad, were not expressed, the cells were still treated with peptides 40Gap27, 37/43Gap27, 45Gap27 (P-Cx) or Anti-N-Cadherin antibody (AN-C), which targeted Cx40, Cx43, and Cx45 or N-cad junctions, respectively, to completely inhibit the interaction between cardiomyocytes and fibroblasts (Figure 2.3). When the cells were treated with the drugs, their organizational response to cyclic strain was not significantly different from those observed in the cultures with no drugs (Figure 2.1E-J & Figure 2.3A-F). However, there were subtle differences observed at densities with low amounts of cardiomyocytes where the OOP

was slightly lower compared to the controls (Figure 2.3E, fractions <0.2). Overall, we were not able to see any significant differences in response to the drugs in the OOP of cardiomyocytes and fibroblasts in any of the densities (Figure 2.3E-F).

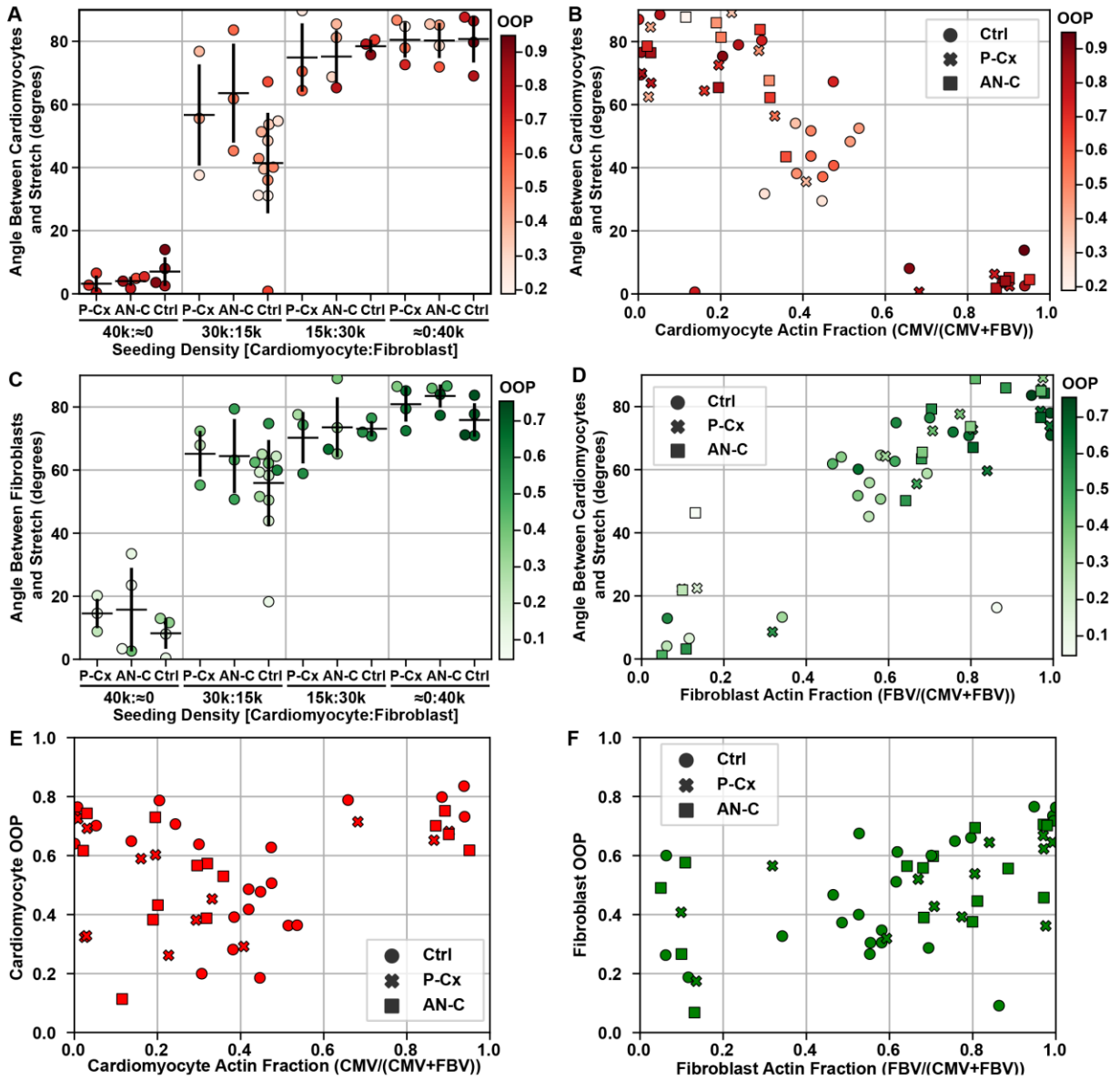

Figure 2.3 Co-cultures treated with drugs. (A) The average and standard deviation of the angle between the cardiomyocyte actin director and stretch director for each experimental seeding density. (B) The angle between the cardiomyocyte actin director and stretch director for the measured cell type actin fraction i.e., the total number of cardiomyocyte actin vectors divided by the total number actin vectors. (C) The average and standard deviation of the angle between

the fibroblast actin director and stretch director for each experimental seeding density. (D) The angle between the fibroblast actin director and stretch director for the measured cell type actin fraction i.e., the total number of fibroblast actin vectors divided by the total number actin vectors. (E) Cardiomyocyte OOP as a function of actin fraction. (F) Fibroblast OOP as a function of actin fraction. In A-F, each point represents a single well, which is colored by the actin OOP for cardiomyocytes (A,B,E) or fibroblasts (C,D,F). In A and C, horizontal bars indicate groups with significantly different means ($p<0.05$).

DISCUSSION

In this work, we investigated cardiac tissue reorganization by examining co-cultures of the two dominant cell types in the myocardium, fibroblasts and cardiomyocytes, under the influence of cyclic strain to model both the cellular composition of the heart in health and pathology as well as the cardiac mechanical environment (Table 2.1)[1–3]. In order to measure the cell type specific organization, we developed an image processing pipeline to automatically classify images of tissues stained with α-actinin and to use the classification labels to separate the actin belonging to fibroblasts and striated myocytes[45]. With the novel ability to automatically quantify the organization of actin for each individual cell types, we then evaluated cell type specific structure using organizational metrics such as the OOP and the director (Figure 2.1E-J & Figure 2.3A-F).

The heart is a complex organ that consists of many different cell types and structures, which makes it difficult to fully replicate *in vitro*[1–3,46-50]. Thus, separating and simplifying the components that contribute to heart function would facilitate the investigation of vital processes such as cardiac remodeling and repair. In this spirit, our work utilized two of the most abundant cell types in the heart, fibroblasts andcardiomyocytes[1–3,46], to procure a general understanding of how organization in the heart is determined and transformed with and without pathology. Together, with the application of mechanical cyclic strain to these co-cultures, a simplified yet representative model of the myocardial environment was developed. In order to create a robust model, the experiments

incorporated various densities to capture physiological relevant events in the heart (Table 2.1)[6,11,51-53].

With a range of different seeding densities, we were able to replicate organization that mimics healthy heart tissue and organization with low OOP that mimics what happens during fibrosis (Figure 2.1E-J). However, the densities at which the organization of healthy heart tissue occur differs between our system and the *in vivo* environment. In the ventricles of the human heart, there is approximately twice the amount of cardiomyocytes when compared to fibroblasts[1–3,46]. Yet, the familiar organization found in healthy heart tissue did not appear until cardiomyocytes occupied approximately 80% of the culture *in vitro* (Figure 2.1I fractions >0.8)[7–9]. One of the possible reasons for the difference observed in the cellular composition *in vitro* is that the heart has a laminar hierarchy, which consists of layers or "sheets" of muscle a few myocytes thick connected by collagen fibers[47-49]. As a result, the cells within the heart are surrounded by extracellular matrix proteins and others cells in all directions, increasing both extracellular matrix and cell-cell contact, respectively[47-49]. Even though monolayer cultures of cardiomyocytes and fibroblasts incorporated physiologically relevant densities and are representative of a single sheet within the laminar hierarchy (Table 2.1), the reduction of cell-cell or extracellular matrix contact could potentially explain the shift in the organizational order observed (Figure 2.1E-J). On the other hand, though the density at which organization of healthy heart tissue occurred was shifted *in vitro*, organization correlating to fibrotic tissue appeared at the expected density where fibroblasts occupied 65% of the culture (Figure 2.1I-J). Based on our results, in order to model healthy or fibrotic heart tissue *in vitro*, approximate cell ratios of 5:1 and 1:2, respectively, should be utilized as these densities mimic the organization found *in vivo* (Figure 2.1I).

As cardiac cells are known to respond to mechanical strain[25,30,34,54], intercellular junctions that mechanically and electrically couple cells to one another were potentially a factor that could play an influential role in controlling fibroblast and cardiomyocyte alignment in the heart. Within the heart, the predominant gap and adherens junctions are N-cad, Cx40, Cx43, and Cx45 depending on the area of the heart being examined[1,6,26,36–40]. Our experiments with cardiac cells originating from the ventricles of the heart confirmed the expression of Connexin 40 and 43 with immunofluorescence imaging and western blotting (Figure 2.2), which is consistent with previous studies[55-56]. Interestingly, studies have shown that disrupting or blocking these junctions can inhibit cell-cell contact, adhesion, and signaling between cells[1,26,36,39,41,42]. Yet, in our experiments, using drugs to inhibit intercellular junctions of N-cad, Cx40, Cx43, and Cx45 resulted in no differences in the organization when compared to controls (Figure 2.1 & Figure 2.3). Our results indicate that Cx40, Cx43, Cx45, and N-cad did not have a dominant effect on the reorganization of cardiomyocytes and fibroblasts in monolayer co-cultures exposed to cyclic strain. However, there are a few limitations that should be considered when interpreting these results such as the effectiveness of Gap27 in comparison to knockdown studies and the differences in the abundance of intercellular junctions between monocultures and the laminar hierarchy of the heart[47-49,57,58].

With the novel image processing pipeline created for this work[45], it is now possible to classify and quantify the organization of different cell types found in the heart. The cardiomyocytes and fibroblasts exhibited influences on the organization of one another when exposed to cyclic strain, especially in cases where the presence of one of the cell types was particularly dominant. However, in the intermediate densities, the influence exerted by the prevalent cell type was not dominant enough to dictate organization fully with each cell type trying to organize based on its preference. Furthermore, our data indicated that cell-cell contact via intercellular junctions was not

a dominant mechanism that contributes to the organization of monolayered co-cultures of cardiomyocytes and fibroblasts. In this work, we were able to replicate the organization or lack thereof observed in healthy and fibrotic heart tissue, respectively, through the utilization of different cardiac cell types and mechanical strain. By establishing the cell ratios that would generate tissue resembling healthy or fibrotic cardiac tissue, we provide future models with working densities that could be used to further study cardiac repair and reorganization *in vitro*.

ACKNOWLEDGEMENTS

The authors would like to thank Hamza Atcha and Vijaykumar S. Meli for their help in western blotting. We would also like to thank Professor Samuel Safran, Professor Eran Bouchbinder, and Avraham Moriel for discussions related to this work.

FUNDING

This work was funded by the National Institute of Health (NIH): National Institute T32 Training Grant in Cardiovascular Applied Research and Entrepreneurship (5T32 HL116270-3), National Institute of Biomedical Imaging and Bioengineering R03 EB028605, and S10 Equipment grant (confocal microscope) 1S10OD025064. This work was also (partially) supported by an NSF grant, DMS1763272, and a grant from the Simons Foundation (594598). The funders had no role in the study design, data collection, data analysis, interpretation of the data, writing of the manuscript, or decision for publication.

MATERIALS & METHODS

Cardiomyocyte and fibroblast harvest

All animals for the study were treated according to the Institutional Animal Care and Use Committee of University of California, Irvine guidelines (IACUC Protocol No. 2013-3093). The recommendations of the NIH Guide for the Care and Use of Laboratory Animals were followed and the experiments were also in accordance with existing federal (9 CFR Parts 1, 2, & 3), state, and city laws and regulations governing the use of animals in research and teaching. Harvest was done with a previously established protocol[59]. Briefly, 2 day old neonatal Sprague Dawly rat pups (Charles River Laboratories Wilmington, MA) were euthanized by decapitation and the ventricular myocardium were extracted. Cardiomyocytes were then isolated from the ventricular tissue as described previously[60-63]. Ventricular tissue were then washed with Hanks' balanced salt solution buffer (HBSS; Life Technologies, Carlsbad, CA) and then incubated overnight (12 hr) at 4°C in a 1 mg/mL trypsin solution (Sigma Aldrich, Inc., Saint Louis, MO) dissolved in HBSS. After incubation, the trypsin solution was neutralized with warm M199 culture media (Invitrogen, Carlsbad, CA) supplemented with 10% fetal bovine serum (FBS; ThermoFisher, Grand Island, NY). The tissue was then washed four times with 1 mg/mL collagenase (Worthington Biochemical Corporation, Lakewood, NJ) dissolved in HBSS. The isolated cell solutions were centrifuged at 1200 rpm for 10 min and resuspended in chilled HBSS, before being centrifuged again at 1200 rpm for 10 min. The cells were then resuspended in warm 10% FBS M199 culture media and purified through three consecutive preplates. The final solution of cardiomyocytes were collected and then seeded at the required densities with or without fibroblasts (Table 2.1). Cardiac fibroblasts remaining within the preplates are kept and passaged once for experiments. The cardiac fibroblasts were cultured in the same 10% FBS M199 culture media. The preplates were then passaged at 80-100% confluency, using 0.05% Trypsin (Fisher Scientific, Hanover Park, IL). Once confluent, the

cardiac fibroblasts were trypsinized, collected, counted, and seeded at the specified densities (Table 2.1).

Stretcher Experiments

MechanoCulture FX-2 (CellScale, CDN), stretcher device, was used to apply cyclic stretch to the cells. The actuator was programmed to execute manufacturer specified 15% uniaxial cyclic stretch at 1 Hz for 48 hr. Seeding the stretcher followed a previously established protocol[24]. Briefly, the wells were initially washed and primed with Phosphate Buffered Saline (PBS, ThermoFisher, Grand Island, NY). A 0.05mg/mL fibronectin solution was then added to each well (Fisher Scientific, Hanover Park, IL) and incubated overnight at 4°C. The wells were washed once more with PBS to remove excess fibronectin before adding a 300 μL solution of cells, culturing media, and drug depending on the experimental condition. The cells were placed inside an incubator with 5% CO2 at 37°C for the duration of the experiment. After 30 min post seeding, the stretching protocol was initiated at the specified 15% uniaxial cyclic stretch at 1 Hz for 48hr. At the 24 hr time point, the media was changed with culture media with or without drugs depending on the experimental condition. Once the whole 48 hr cycle was completed, the cells were then fixed and immunostained.

Inhibiting intercellular junctions

To inhibit Connexin 40, Connexin 43, Connexin 45, and N-Cadherin intercellular formations, 40Gap27 (sequence SPRTEKNVFIV), 37/43Gap27 (sequence SRPTEKTIFII), 45Gap27 (sequence SPRTEKTIFLL), and Anti-N-Cadherin antibody (Millipore Sigma, St. Louis, MO) were used, respectively. Each of the peptides and the antibody were used at the concentrations of 300 μM. The peptides and antibody where dissolved in 10% FBS M199 media. A solution with

similar concentrations respective to each condition was used for the media change after the first 24 hr of stretch.

Fixing and Immunostaining

The cells were fixed with a solution of 4% paraformaldehyde (VWR, Radnow, PA) and 0.05% Triton X-100 (Sigma-Aldrich, Saint Louis, MO) for 15 min. Each well was washed three times with PBS for 5 min after fixing. The cultures were then stained for nuclei (4,6-Diamidino-2-Phenylindole Dihydrochloride, DAPI, ThermoFisher, Grand Island, NY), actin (Alexa Fluor 488 Phalloidin, ThermoFisher, Grand Island, NY), and sarcomeric α-actinin (Mouse Monoclonal Anti-α–actinin; Sigma Aldrich, Inc., St. Louis, MO). The wells were then washed with PBS three times to remove excess stain. Secondary staining was completed with goat anti-rabbit IgG secondary antibodies (Alexa Fluor 633, ThermoFisher, Grand Island, NY). The wells were once more washed 3 times with PBS to remove excess staining. Afterwards, the wells were punched out with a square hole puncher and mounted onto glass microscope slides. ProLong Gold Antifade Mountant (ThermoFisher, Grand Island, NY) was applied and a rectangular microglass coverslip was placed on top to cover and seal the sample. Connexin 43 staining followed a similar protocol with just the addition of primary Connexin 43 Antibody (Cell Signaling, Danvers, MA) and goat anti-Mouse IgG secondary antibody (Cyanine5, ThermoFisher, Grand Island, NY).

Imaging and Data Acquisition

The samples were mounted at 90° and imaged with an IX-83 inverted motorized microscope (Olympus America, Center Valley, PA). Images were taken using an UPLFLN 40x oil immersion objective (Olympus America, Center Valley, PA) and a digital CCD camera ORCA-R2 C10600-10B (Hamamatsu Photonics, Shizuoka Prefecture, Japan). Ten fields of views

randomly selected for each sample and imaged at 40x magnification (6.22 μm/pixel). Connexin 43 images were obtained with the Olympus Fluoview FV3000 microscope (Olympus America, Center Valley, PA) also using a UPLSAPO 40x silicone oil immersion objective (Olympus America, Center Valley, PA).

Western Blotting

The western blot was done with a previously established protocol[64-65]. Briefly, the cells were washed with PBS once before they were exposed to a solution of RIPA lysis buffer and 1% protease inhibitor (ThermoFisher, Grand Island, NY). Twenty micrograms of the collected lysis solution was added to equal amounts of Laemmli buffer supplemented with 5% 2-mercaptoethanol and boiled at 95°C for 10 min before loading into a well of 4–15% mini-PROTEANTM precast gels (Bio-Rad, Hercules, California). When gel electrophoresis was completed, the proteins were blotted onto nitrocellulose membranes using the iBlot dry blotting system (ThermoFisher, Grand Island, NY). After electroblotting, the blots were blocked overnight at 4°C using 5% nonfat milk. The blot was then stained for 1 hr at RT with Connexin 40 polyclonal antibody (ThermoFisher), Connexin 43 antibody (Cell Signaling), 45 Polyclonal Antibody (ThermoFisher), and Monoclonal Anti-N-Cadherin antibody (Sigma Aldrich) as primaries. After the first incubation with primaries, TBST was used to wash the blots for 15 minutes before further incubation with horseradish peroxidase–conjugated secondary for 1 hr at RT. The blots were washed once more with TBST for 15 min after secondaries. For imaging, the blots were incubated in SuperSignal West Femto Maximum Sensitivity Substrate (ThermoFisher, Grand Island, NY) for 5 min before imaging the blot using Bio-Rad ChemiDoc XRS+ with Image Lab software.

Statistical Analysis

To determine statistical significance, one-way analysis of variance (ANOVA) with Tukey's Test was performed in Python 3.7.7 using the module, *statsmodels*. A p-value less than 0.05 was considered significant.

Cell Type Classifier

Development of the image classification pipeline, nuclei segmentation and cell type classification, and cell type orientation analysis was done by Tessa Altair Morris[45], while in the laboratory of Anna Grosberg, Ph.D. at the University of California, Irvine.

REFERENCES

1. Meghan B Knight, Anna Grosberg, and Megan L McCain. In Vitro Tools for Quantifying Structure–Function Relationships in Cardiac Myocyte Cells and Tissues. In *Cardiac Cytoarchitecture*, pages 15–39.Springer, 2015.
2. HW Vliegen, A Van der Laarse, CJ Cornelisse, and F Eulderink. Myocardial changes in pressure overload-induced left ventricular hypertrophy: A study on tissue composition, polyploidization and multinucleation. *European heart journal*, 12(4):488–494, 1991.
3. Indroneal Banerjee, John W Fuseler, Robert L Price, Thomas K Borg, and Troy A Baudino. Determination of cell types and numbers during cardiac development in the neonatal and adult rat and mouse. *American Journal of Physiology-Heart and Circulatory Physiology*, 293(3):H1883–H1891, 2007.
4. C A Souders, S L K Bowers, and T A Baudino. Cardiac Fibroblast The Renaissance Cell. *Circulation Research*, 105(12):1164–1176, 2009. ISSN 0009-7330. doi: 10.1161/Circresaha.109.209809.
5. Peter Kohl and Patrizia Camelliti. Fibroblast–myocyte connections in the heart. *Heart Rhythm*, 9(3):461–464, 2012.
6. Patrizia Camelliti, Thomas K. Borg, and Peter Kohl. Structural and functional characterisation of cardiac fibroblasts, 2005. ISSN 00086363.
7. Richard A Lasher, Aric Q Pahnke, Jeffrey M Johnson, Frank B Sachse, and Robert W Hitchcock. Electrical stimulation directs engineered cardiac tissue to an age-matched native phenotype. *Journal of tissue engineering*, 3(1):2041731412455354, 2012.
8. Peter Kohl and Robert G Gourdie. Fibroblast–myocyte electrotonic coupling: does it occur in native cardiac tissue? *Journal of molecular and cellular cardiology*, 70:37–46, 2014.
9. Ana Rita M.P. Santos, Yongjun Jang, Inwoo Son, Jongseong Kim, and Yongdoo Park. Recapitulating cardiac structure and function in vitro from simple to complex engineering, 2021. ISSN 2072666X.
10. Carlo Alberto Beltrami, Nicoletta Finato, Maurizio Rocco, Giorgio A. Feruglio, Cesare Puricelli, Elena Cigola, Edmund H. Sonnenblick, Giorgio Olivetti, and Piero Anversa. The cellular basis of dilated cardiomyopathy in humans. *Journal of Molecular and Cellular Cardiology*, 27(1):291–305, 1995. ISSN00222828. doi: 10.1016/S0022-2828(08)80028-4.
11. Patrizia Camelliti, Gerard P. Devlin, Kenneth G. Matthews, Peter Kohl, and Colin R. Green. Spatially and temporally distinct expression of fibroblast connexins after sheep ventricular infarction. *Cardiovascular Research*, 62(2):415–425, 2004. ISSN 00086363. doi: 10.1016/j.cardiores.2004.01.027.
12. Claudio Humeres and Nikolaos G Frangogiannis. Fibroblasts in the infarcted, remodeling, and failing heart. JACC: Basic to *Translational Science*, 4(3):449–467, 2019.
13. Wei Chen and Nikolaos G Frangogiannis. Fibroblasts in post-infarction inflammation and cardiac repair. *Biochimica et Biophysica Acta (BBA)-Molecular Cell Research*, 1833(4):945–953, 2013.
14. Ronald B. Driesen, Fons K. Verheyen, Petra Dijkstra, Fred Thoné, Jack P. Cleutjens, Marie Hélène Lenders, Frans C.S. Ramaekers, and Marcel Borgers. Structural remodelling of cardiomyocytes in the border zone of infarcted rabbit heart. *Molecular and Cellular Biochemistry*, 302(1-2), 2007. ISSN 03008177.doi: 10.1007/s11010-007-9445-2.
15. Eeva Palojoki, Antti Saraste, Anders Eriksson, Kari Pulkki, Markku Kallajoki, Liisa Maria Voipio-Pulkki, and Ilkka Tikkanen. Cardiomyocyte apoptosis and ventricular remodeling

after myocardial infarction in rats. *American Journal of Physiology - Heart and Circulatory Physiology*, 280(6 49-6), 2001.ISSN 03636135. doi: 10.1152/ajpheart.2001.280.6.h2726.
16. Susan Van Noorden, E. G.J. Olsen, and A. G.E. Pearse. Hypertrophic obstructive cardiomyopathy, a histological, histochemical, and ultrastructural study of biopsy material. *Cardiovascular Research*, 5(1), 1971. ISSN 00086363. doi: 10.1093/cvr/5.1.118.
17. V. J. Ferrans, A. G. Morrow, and W. C. Roberts. Myocardial ultrastructure in idiopathic hypertrophic subaortic stenosis. A study of operatively excised left ventricular outflow tract muscle in 14 patients. *Circulation*, 45(4), 1972. ISSN 00097322. doi: 10.1161/01.CIR.45.4.769.
18. B. J. Maron, T. J. Anan, and W. C. Roberts. Quantitative analysis of the distribution of cardiac muscle ell disorganization in the left ventricular wall of patients with hypertonic cardiomyopathy. *Circulation*, 63(4), 1981. ISSN 00097322. doi: 10.1161/01.CIR.63.4.882.
19. Sara McMahan, Alan Taylor, Katherine M. Copeland, Zui Pan, Jun Liao, and Yi Hong. Current advances in biodegradable synthetic polymer based cardiac patches, 2020. ISSN 15524965.
20. Nadav Noor, Assaf Shapira, Reuven Edri, Idan Gal, Lior Wertheim, and Tal Dvir. 3D Printing of Personalized Thick and Perfusable Cardiac Patches and Hearts. *Advanced Science*, 6(11), 2019. ISSN21983844. doi: 10.1002/advs.201900344.
21. Rajesh Lakshmanan, Uma Maheswari Krishnan, and Swaminathan Sethuraman. Living cardiac patch: The elixir for cardiac regeneration, 2012. ISSN 14712598.
22. Anna Grosberg, Patrick W Alford, Megan L McCain, and Kevin Kit Parker. Ensembles of engineered cardiac tissues for physiological and pharmacological study: heart on a chip. *Lab on a chip*, 11(24):4165–4173, 2011.
23. Yimu Zhao, Naimeh Rafatian, Erika Y. Wang, Nicole T. Feric, Benjamin F.L. Lai, Ericka J. Knee-Walden, Peter H. Backx, and Milica Radisic. Engineering microenvironment for human cardiac tissue assembly in heart-on-a-chip platform. *Matrix Biology*, 85-86, 2020. ISSN 15691802. doi: 10.1016/j.matbio.2019.04.001.
24. Richard DH Tran, Mark Siemens, Cecilia HH Nguyen, Alexander R Ochs, Michael V Zaragoza, and Anna Grosberg. The effect of cyclic strain on human fibroblasts with lamin a/c mutations and its relation to heart disease. *Journal of Biomechanical Engineering*, 142(6), 2020.
25. T Matsuda, K Takahashi, T Nariai, T Ito, T Takatani, Y Fujio, and J Azuma. N-cadherin-mediated cell adhesion determines the plasticity for cell alignment in response to mechanical stretch in cultured cardiomyocytes. *Biochem Biophys Res Commun*, 326(1):228–232, 2005. ISSN 0006-291X (Print) 0006-291X (Linking). doi: 10.1016/j.bbrc.2004.11.019. URLhttp://www.ncbi.nlm.nih.gov/pubmed/15567175.
26. Aida Salameh, Anne Wustmann, Sebastian Karl, Katja Blanke, Daniel Apel, Diana Rojas-Gomez, Heike Franke, Friedrich W. Mohr, Jan Janousek, and Stefan Dhein. Cyclic mechanical stretch induces cardiomyocyte orientation and polarization of the gap junction protein connexin43. *Circulation Research*, 106(10):1592–1602, 2010. doi: 10.1161/CIRCRESAHA.109.214429.
27. Alexandra M Greiner, Hao Chen, Joachim P Spatz, and Ralf Kemkemer. Cyclic tensile strain controls cell shape and directs actin stress fiber formation and focal adhesion alignment in spreading cells. *PloS one*, 8(10):e77328, 2013.
28. Uta Faust, Nico Hampe, Wolfgang Rubner, Norbert Kirchgeßner, Sam Safran, Bernd Hoffmann, and Rudolf Merkel. Cyclic stress at mHz frequencies aligns fibroblasts in

direction of zero strain. *PLoS ONE*, 6(12), 2011. ISSN 19326203. doi: 10.1371/journal.pone.0028963.
29. Uta Faust, Nico Hampe, Wolfgang Rubner, Norbert Kirchgessner, Sam Safran, Bernd Hoffmann, and Rudolf Merkel. Cyclic stress at mhz frequencies aligns fibroblasts in direction of zero strain. *PloS one*, 6(12):e28963, 2011.
30. R.D.H. Tran, M. Siemens, C.H.H. Nguyen, A.R. Ochs, M.V. Zaragoza, and A. Grosberg. The effect of cyclic strain on human fibroblasts with lamin a/c mutations and its relation to heart disease. *Journal of Biomechanical Engineering*, 142(6), 2020. ISSN 15288951. doi: 10.1115/1.4044091.
31. Ulrich S. Schwarz and Samuel A. Safran. Physics of adherent cells. *Reviews of Modern Physics*, 85(3), 2013. ISSN 00346861. doi: 10.1103/RevModPhys.85.1327.
32. Rumi De, Assaf Zemel, and Samuel A. Safran. Do cells sense stress or strain? measurement of cellular orientation can provide a clue. *Biophysical Journal*, 94(5):L29–L31, 3 2008. ISSN 15420086. doi: 10.1529/biophysj.107.126060.
33. Rumi De and Samuel A. Safran. Dynamical theory of active cellular response to external stress. *Rev. Mod. Phys*, 78(3), 9 2008. ISSN 15393755. doi: 10.1103/PhysRevE.78.031923.
34. A M Greiner, H Chen, J P Spatz, and R Kemkemer. Cyclic tensile strain controls cell shape and directs actin stress fiber formation and focal adhesion alignment in spreading cells. *PLoS One*, 8(10):e77328, 2013. ISSN 1932-6203 (Electronic) 1932-6203 (Linking). doi: 10.1371/journal.pone.0077328. URL http://www.ncbi.nlm.nih.gov/pubmed/24204809.
35. Stefan Dhein, Anna Schreiber, Sabine Steinbach, Daniel Apel, Aida Salameh, Franziska Schlegel, Martin Kostelka, Pascal M. Dohmen, and Friedrich Wilhelm Mohr. Mechanical control of cell biology. Effects of cyclic mechanical stretch on cardiomyocyte cellular organization. *Progress in Biophysics and Molecular Biology*, 115(2-3):93–102, 2014. ISSN 00796107. doi: 10.1016/j.pbiomolbio.2014.06.006. URLhttp://dx.doi.org/10.1016/j.pbiomolbio.2014.06.006.
36. Peng Zhang, Jialin Su, and Ulrike Mende. Cross talk between cardiac myocytes and fibroblasts: from multiscale investigative approaches to mechanisms and functional consequences. *American Journal of Physiology-Heart and Circulatory Physiology*, 303(12):H1385–H1396, 2012.
37. Carolina Vasquez, Poornima Mohandas, Karen L. Louie, Najate Benamer, Ashwini C. Bapat, and Gregory E. Morley. Enhanced fibroblast-myocyte interactions in response to cardiac injury. *Circulation Research*, 107(8), 2010. ISSN 00097330. doi: 10.1161/CIRCRESAHA.110.227421.
38. Thomas Desplantez, Emmanuel Dupont, Nicholas J. Severs, and Robert Weingart. Gap junction channels and cardiac impulse propagation, 2007. ISSN 00222631.
39. Yang Li, Chelsea D. Merkel, Xuemei Zeng, Jonathon A. Heier, Pamela S. Cantrell, Mai Sun, Donna B. Stolz, Simon C. Watkins, Nathan A. Yates, and Adam V. Kwiatkowski. The N-cadherin interactome in primary cardiomyocytes as defined using quantitative proximity proteomics. *Journal of cell science*, 132(3), 2019. ISSN 14779137. doi: 10.1242/jcs.221606.
40. Jiahn-Chun Wu, Ru-Yin Tsai, and Tun-Hui Chung. Role of catenins in the development of gap junctions in rat cardiomyocytes. *Journal of cellular biochemistry*, 88(4):823–835, 2003.
41. Troy A. Baudino, Alex McFadden, Charity Fix, Joshua Hastings, Robert Price, and Thomas K. Borg. Cell patterning: Interaction of cardiac myocytes and fibroblasts in three-dimensional culture. *Microscopy and Microanalysis*, 14(2):117–125, 2008. ISSN 14319276. doi: 10.1017/S1431927608080021.

42. Jason Pellman, Jing Zhang, and Farah Sheikh. Myocyte-fibroblast communication in cardiac fibrosis and arrhythmias: Mechanisms and model systems. *Journal of Molecular and Cellular Cardiology*, 94(3):22–31, 2016. ISSN 10958584. doi: 10.1016/j.yjmcc.2016.03.005.
43. Charlotte Mehlin Sorensen, Max Salomonsson, Thomas Hartig Braunstein, Morten Schak Nielsen, andNiels Henrik Holstein-Rathlou. Connexin mimetic peptides fail to inhibit vascular conducted calcium responses in renal arterioles. *American Journal of Physiology - Regulatory Integrative and Comparative Physiology*, 295(3), 2008. ISSN 15221490. doi: 10.1152/ajpregu.00491.2007.
44. Amir Schajnovitz, Tomer Itkin, Gabriele D'Uva, Alexander Kalinkovich, Karin Golan, Aya Ludin, Dror Cohen, Ziv Shulman, Abraham Avigdor, Arnon Nagler, Orit Kollet, Rony Seger, and Tsvee Lapidot. CXCL12 secretion by bone marrow stromal cells is dependent on cell contact and mediated by connexin-43 and connexin-45 gap junctions. *Nature Immunology*, 12(5), 2011. ISSN 15292908. doi:10.1038/ni.2017.
45. Morris, Tessa Altair. Computational and Image Analysis Techniques for Quantitative Evaluation of Striated Muscle Tissue Architecture. 2021. University of California, Irvine, PhD dissertation.
46. Pingzhu Zhou and William T. Pu. Recounting cardiac cellular composition, 2016. ISSN 15244571.
47. I. J. LeGrice, B. H. Smaill, L. Z. Chai, S. G. Edgar, J. B. Gavin, and P. J. Hunter. Laminar structure of the heart: Ventricular myocyte arrangement and connective tissue architecture in the dog. *American Journal of Physiology - Heart and Circulatory Physiology*, 269(2 38-2), 1995. ISSN 03636135. doi: 10.1152/ajpheart.1995.269.2.h571.
48. I. J. LeGrice, P. J. Hunter, and B. H. Smaill. Laminar structure of the heart: A mathematical model. *American Journal of Physiology - Heart and Circulatory Physiology*, 272(5 41-5), 1997. ISSN 03636135. doi:10.1152/ajpheart.1997.272.5.h2466.
49. T. F. Robinson, M. A. Geraci, E. H. Sonnenblick, and S. M. Factor. Coiled perimysial fibers of papillary muscle in rat heart: Morphology, distribution, and changes in configuration. *Circulation Research*, 63(3), 1988. ISSN 00097330. doi: 10.1161/01.RES.63.3.577.
50. Robert H. Anderson, Reza Razavi, and Andrew M. Taylor. Cardiac anatomy revisited, 2004. ISSN00218782.
51. Peter Kohl and Robert G. Gourdie. Fibroblast-myocyte electrotonic coupling: Does it occur in native cardiac tissue?, 2014. ISSN 10958584.
52. Arti V. Shinde and Nikolaos G. Frangogiannis. Fibroblasts in myocardial infarction: A role in inflammation and repair, 2014. ISSN 10958584.
53. Claudio Humeres and Nikolaos G. Frangogiannis. Fibroblasts in the Infarcted, Remodeling, and Failing Heart, 2019. ISSN 2452302X.
54. A Salameh, A Wustmann, S Karl, K Blanke, D Apel, D Rojas-Gomez, H Franke, F W Mohr, J Janousek, and S Dhein. Cyclic mechanical stretch induces cardiomyocyte orientation and polarization of the gap junction protein connexin43. *Circulation Research*, 106(10):1592–1602, 2010. ISSN 1524-4571 (Electronic) 0009-7330 (Linking). doi: 10.1161/CIRCRESAHA.109.214429. URL http://www.ncbi.nlm.nih.gov/pubmed/20378856.
55. Xianming Lin, Joanna Gemel, Aaron Glass, Christian W. Zemlin, Eric C. Beyer, and Richard D. Veenstra. Connexin40 and connexin43 determine gating properties of atrial gap junction channels. *Journal of Molecular and Cellular Cardiology*, 48(1), 2010. ISSN 00222828. doi: 10.1016/j.yjmcc.2009.05.014.

56. Aida Salameh, Katja Blanke, and Ingo Daehnert. Role of connexins in human congenital heart disease: The chicken and egg problem, 2013. ISSN 16639812.
57. Chen Li, Qingli Meng, Xinfeng Yu, Xian Jing, Pingxiang Xu, and Dali Luo. Regulatory effect of con-nexin 43 on basal ca2+ signaling in rat ventricular myocytes. *PLoS ONE*, 7(4), 2012. ISSN 19326203.doi: 10.1371/journal.pone.0036165.
58. Chrysovalantou Faniku, Erin O'Shaughnessy, Claire Lorraine, Scott R. Johnstone, Annette Graham, Sebastian Greenhough, and Patricia E.M. Martin. The connexin mimetic peptide Gap27 and Cx43-knockdown reveal differential roles for connexin43 in wound closure events in skin model systems. *International Journal of Molecular Sciences*, 19(2), 2018. ISSN 14220067. doi: 10.3390/ijms19020604.
59. Tessa Altair Morris, Jasmine Naik, Kirby Sinclair Fibben, Xiangduo Kong, Tohru Kiyono, Kyoko Yokomori, and Anna Grosberg. Striated myocyte structural integrity: Automated analysis of sarcomeric z-discs. *PLoS computational biology*, 16(3):e1007676, 2020.
60. Anna Grosberg, Po-Ling Kuo, Chin-Lin Guo, Nicholas A Geisse, Mark-Anthony Bray, William J Adams, Sean P Sheehy, and Kevin Kit Parker. Self-organization of muscle cell structure and function. *PLoS computational biology*, 7(2):e1001088, 2011.
61. Nancy K Drew, Mackenzie A Eagleson, Danny B Baldo Jr, Kevin Kit Parker, and Anna Grosberg. Metrics for assessing cytoskeletal orientational correlations and consistency. *PLoS computational biology*, 11(4):e1004190, 2015.
62. Nancy K Drew, Nicholas E Johnsen, Jason Q Core, and Anna Grosberg. Multiscale characterization of engineered cardiac tissue architecture. *Journal of biomechanical engineering*, 138(11):111003, 2016.
63. Meghan B Knight, Nancy K Drew, Linda A McCarthy, and Anna Grosberg. Emergent global contractile force in cardiac tissues. *Biophysical journal*, 110(7):1615–1624, 2016.
64. Vijaykumar S. Meli, Hamza Atcha, Praveen Krishna Veerasubramanian, Raji R. Nagalla, Thuy U. Luu, Esther Y. Chen, Christian F. Guerrero-Juarez, Kosuke Yamaga, William Pandori, Jessica Y. Hsieh, Timothy L. Downing, David A. Fruman, Melissa B. Lodoen, Maksim V. Plikus, Wenqi Wang, and Wendy F.Liu. YAP-mediated mechanotransduction tunes the macrophage inflammatory response. *Science Advances*, 6(49), 2020. ISSN 23752548. doi: 10.1126/sciadv.abb8471.
65. Hamza Atcha, Amit Jairaman, Jesse R. Holt, Vijaykumar S. Meli, Raji R. Nagalla, Praveen Krishna Veerasubramanian, Kyle T. Brumm, Huy E. Lim, Shivashankar Othy, Michael D. Cahalan, Medha M. Pathak, and Wendy F. Liu. Mechanically activated ion channel Piezo1 modulates macrophage polarization and stiffness sensing. *Nature Communications*, 12(1), 2021. ISSN 20411723. doi: 10.1038/s41467-021-23482-5.

SUPPLEMENTAL FIGURES

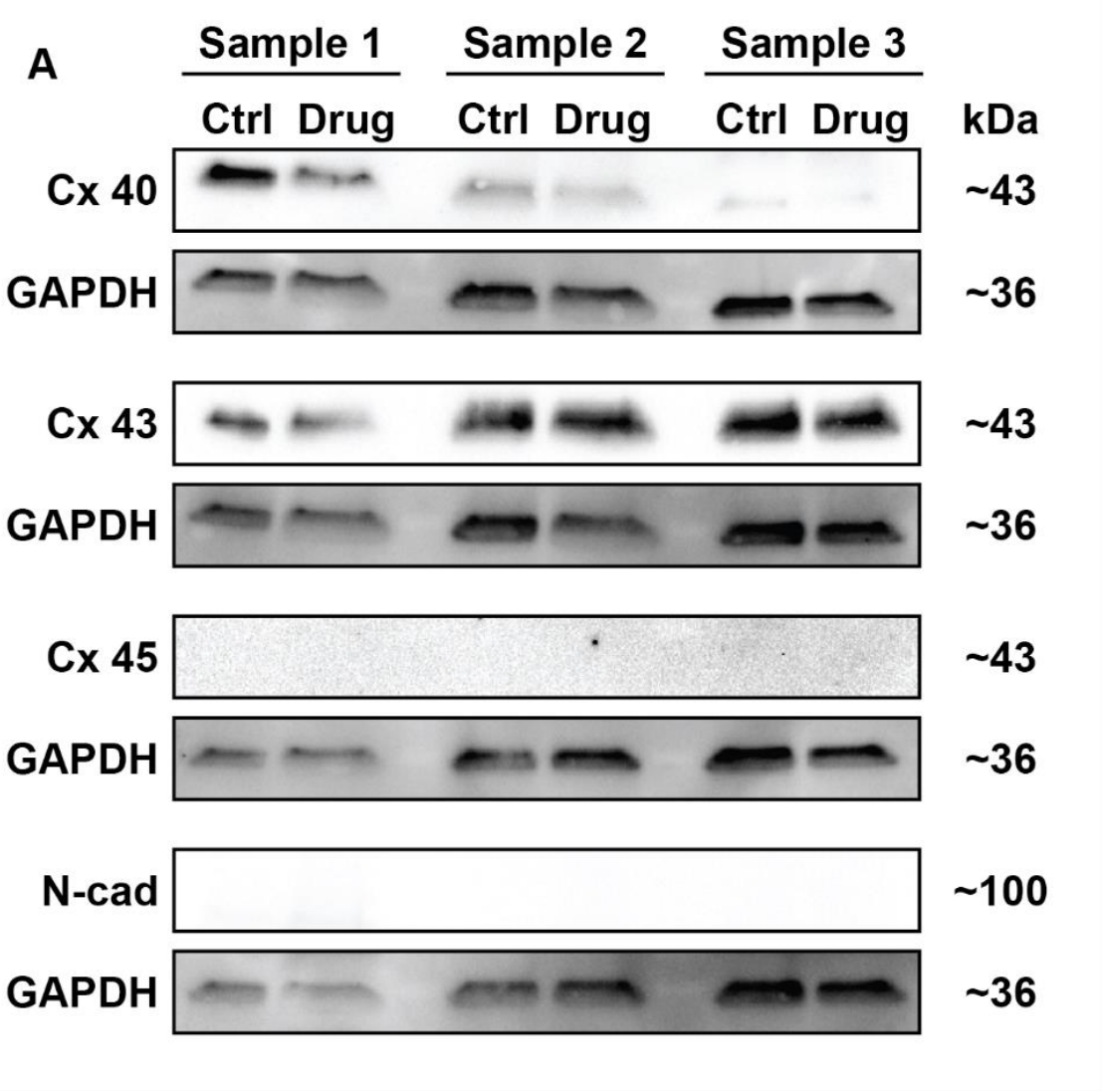

Figure 2.4 Intercellular junction western blots. (A) Western blot of three different experimental runs (Sample 1, 2, and 3) showing expression of each protein with (Drug) and without drugs (Ctrl).

CHAPTER 3

The Effect of Cyclic Strain on Human Fibroblasts with Lamin A/C Mutations and Its Relation to Heart Disease[2]

ABSTRACT

Although mutations in the Lamin A/C gene (LMNA) cause a variety of devastating diseases, the pathological mechanism is often unknown. Lamin A/C proteins play a crucial role in forming a meshwork under the nuclear membrane, providing the nucleus with mechanical integrity and interacting with other proteins for gene regulation. Most LMNA mutations result in heart diseases, including some types that primarily have heart disease as the main pathology. In this study, we used cells from patients with different LMNA mutations that primarily lead to heart disease. Indeed, it is a mystery why a mutation to the protein in every nucleus of the body manifests as a disease of primarily the heart in these patients. Here, we aimed to investigate if strains mimicking those within the myocardial environment are sufficient to cause differences in cells with and without the LMNA mutation. To test this, a stretcher device was used to induce cyclic strain upon cells, and viability/proliferation, cytoskeleton and extracellular matrix organization, and nuclear morphology were quantified. The properties of cells with Hutchinson-Gilford progeria syndrome were found to be significantly different from all other cell lines and were mostly in line with previous findings. However, the properties of cells from patients that primarily had heart diseases were not drastically different when compared to individuals without the LMNA mutation. Our

[2] Tran, Richard D.H. et al. (2020) *Journal of Biomechanical Engineering*

results indicated that cyclic strain alone was insufficient to cause any significant differences that could explain the mechanisms that lead to heart diseases in these patients with LMNA mutations.

Keywords: *Lamin A/C, laminopathies, cyclic strain, heart mechanics, heart disease*

INTRODUCTION

Genetic mutations that affect cellular functions and properties, potentially develop into detrimental diseases in the body. One gene that is known to lead to pathologies, when mutated, is the Lamin A/C gene (*LMNA*) [1, 2]. Lamin A and C, A-type lamins encoded by *LMNA*, are type V intermediate filament proteins present in all nucleated somatic cells in the body [3]. These proteins form a supportive meshwork, known as the nuclear lamina, that provides mechanical and structural support for the nuclear envelope [4]. In addition, A-type lamins interact with nucleoplasm and chromatin proteins allowing them to take part in both gene regulation and mechanical signaling [5-7]. Mutations to *LMNA* have been linked to a wide range of diseases, referred to as laminopathies, affecting multiple tissues and organs systems within the body [1, 2]. Though each mutation variant may affect different parts of the body, most laminopathies are known to be associated with some form of heart disease [1, 2]. Indeed, there are also *LMNA* mutations which primarily lead to heart diseases with no other detrimental pathologies [8-10]. Given that A-type lamins are found in every nucleated cell throughout the body, it is unclear why the heart is specifically vulnerable to the *LMNA* mutation.

Mutations in A-type lamins are known to make cells vulnerable to mechanical perturbations due to the decrease in stiffness and stability of the nuclear lamina [11-14]. For example, an impaired nuclear lamina can result in a loss of cell viability and functionality, especially in mechanically stressed tissues [12]. Indeed, when static strain was applied to cells

with the mutation, increased deformability of the nuclear envelope and a higher percentage of dysmorphic nuclei were observed [12, 13, 15]. Although many parts of the body are exposed to strains, only the heart is subjected to repeated ~1 Hz contractions over a lifetime. Thus, cardiomyocytes are uniquely exposed to non-stop cyclic strain which has not yet been investigated for its effects on cells with the *LMNA* mutation. If the consequences are similar to those observed in static strain, cardiomyocyte functionality and heart activity may also be negatively affected.

To understand the mechanisms leading to heart diseases in laminopathies, we investigated if strains mimicking those in myocardial environment alone are sufficient to demarcate cells with and without the *LMNA* mutation. To study this, skin biopsies were taken from patients with *LMNA* mutations who primarily exhibited heart disease [8-10]. In addition, these were compared to cells from healthy individuals with no mutations and from a patient with Hutchinson-Gilford progeria syndrome (HGPS). Fibroblasts were specifically used as they were observed in a previous study to have functional pathologies *in vitro* [16] and are not normally subjected to cyclic strain. By subjecting these non-stretching cells to cyclic strain and observing the consequences on the nuclei, we can better clarify the role of dynamic mechanical strain in causing heart diseases. Thus, a monolayer of cells was uniaxially and cyclically stretched with magnitudes similar to the heart to investigate the effects on cell viability/proliferation, cytoskeleton and extracellular matrix organization, proportion of dysmorphic nuclei, and nuclear shape [17]. These experiments allowed us to address how the myocardial environment affects cells with the *LMNA* mutation and determine if the observed results were sufficient to explain pathways that lead to heart diseases in laminopathies.

METHODS

Skin Fibroblast Acquisition

Informed consent was obtained and approved by UC Irvine Institutional Review Board (IRB# 2014–1253) for this study. Skin fibroblasts were collected from three families with different *LMNA* mutations: Family A having three individuals with the heterozygous *LMNA* splice-site mutation (c.357-2A>G) [8], Family B having three individuals with the heterozygous *LMNA* nonsense mutation (c.736 C>T, pQ246X) in exon 4 [9], and Family C having three individuals with the heterozygous *LMNA* missense mutation (c.1003C>T, pR335W) in exon 6 [10]. In addition, for each family, fibroblasts were collected from three age and gender matched individuals without the mutation to serve as related negative controls. Unrelated negative control fibroblasts, referred to as donor cells, were purchased from Lonza (catalog# CC-2511) and Coriell (catalog# ND31845, AG14284). HGPS fibroblasts with a heterozygous *LMNA* G608G point mutation were obtained from Coriell Institute for Medical Research (Camden, New Jersey: catalog #AG11513) to serve as a positive control [18]. The individuals with *LMNA* mutations from the families were referred to as Patients. Negative Controls included individuals without mutations from the three families and the donors. For nomenclature, patient (P), control (C), or donor (D) are followed by the family designator (A, B, or C) and the preassigned number of the individual (1, 2, 3, or 4).

Cell Culture

All cell lines were expanded to passage 16 for these experiments. Cells were cultured in media consisting of Minimum Essential Media (MEM, ThermoFisher, Grand Island, NY), 10% Fetal Bovine Serum (FBS, ThermoFisher, Grand Island, NY), and 1% Hyclone Antibiotics Antimycotic solution (AB, GE Life Sciences, Utah). Cells were passaged at 80-100% confluency, using 0.05% Trypsin (Fisher Scientific, Hanover Park, IL).

Stretcher Experiments

MechanoCulture FX-2 (CellScale, CDN), stretcher device, was used for all experiments. The actuator was programmed to execute manufacturer specified 15% uniaxial cyclic stretch at 1 Hz for 24 hours or 20% uniaxial cyclic stretch at 1 Hz for 72 hours depending on the experiment.

The wells were first washed with Phosphate Buffered Saline (PBS, ThermoFisher, Grand Island, NY). A 0.05 mg/mL fibronectin solution was then added to each well (Fisher Scientific, Hanover Park, IL) followed by a two-hour incubation for the adhesion of an isotropic fibronectin monolayer to the silicone well bottoms. After being washed with PBS to remove excess fibronectin, a 300 µL solution of $2.0x10^5$ cells and culturing media was then seeded into each well and allowed to incubate for 24 hours. After incubation, media was changed to a maintenance media consisting of MEM, 2% FBS, and 1% AB to maintain confluency. The stretcher device was then initiated with the desired stretching protocol and placed inside an incubator with 5% CO_2 at 37˚C for the duration of the experiment. For the 72-hour experiments, maintenance media was changed every two days.

Fixing and immunofluorescent staining

The cells were fixed with a solution of 4% paraformaldehyde (VWR, Radnow, PA) and 0.05% Triton X-100 (Sigma-Aldrich, Saint Louis, MO). Once fixed, the cultures were stained for nuclei (4,6-Diamidino-2-Phenylindole Dihydrochloride, DAPI, ThermoFisher, Grand Island, NY), actin (Alexa Fluor 488 Phalloidin, ThermoFisher, Grand Island, NY), and fibronectin (polyclonal rabbit anti-human fibronectin, Sigma-Aldrich, Saint Louis, MO). Secondary staining was done for fibronectin using goat anti-rabbit IgG secondary antibodies (Alexa Fluor 750, ThermoFisher, Grand Island, NY). Afterwards, the wells were punched out with a commercially purchased metal

square hole puncher as high-resolution images could not be obtained through the membrane. The punched-out wells were flipped, mounted onto glass microscope slides with ProLong Gold Antifade Mountant (ThermoFisher, Grand Island, NY), and sealed with clear nail polish around the edges.

Imaging and Data Acquisition

The samples were imaged with an IX-83 inverted motorized microscope (Olympus America, Center Valley, PA). Images were taken using an UPLFLN 40x oil immersion objective (Olympus America, Center Valley, PA) and a digital CCD camera ORCA-R2 C10600-10B (Hamamatsu Photonics, Shizuoka Prefecture, Japan). Ten fields of views randomly selected for each sample and imaged at 40x magnification (6.22 μm/pixel).

MATLAB Analysis

A custom written MATLAB code was used to classify nuclei as normal or dysmorphic and measure nuclear properties [16]. Aspect ratio and area were also simultaneously calculated by the code during the process. Additionally, another in-house set of MATLAB codes were used to quantify the orientation order parameter (OOP) of actin and fibronectin [19].

Statistical Analysis

Unless otherwise specified, statistical analysis was done using analysis of variance (ANOVA) one-way testing with Tukey's method. For non-parametric variables (i.e. nuclei defectiveness), the Kruskal Wallis tests was used followed by Dunn's multiple comparison test. Significance was defined as having a p-value of less than 0.05. Sample sizes for density, OOP, and percentage of defective nuclei were the number of individual wells for each group. Sample sizes

for area and aspect ratio were the total number of individual nuclei for each group. A secondary statistical analysis was also done for area and aspect ratio where sample sizes were the individual patients. A summary of the sample sizes of each statistically tested group and the respective statistical tests for each quantification can be found in Tables 3.1 & 3.2.

RESULTS

Dynamic mechanical stimulation is one of the obvious differences between heart and other tissues in the body. To determine if cyclic strain alone is sufficient to cause issues, fibroblasts from cell lines with a *LMNA* mutation were exposed to simplified myocardial-like strains, 15% strain at 1 Hz for 24 hours. Cells with known *LMNA* mutations leading primarily to heart disease (Patients), cells without *LMNA* mutations (Negative Controls), and HGPS cells (Positive Control) were cyclically stretched and analyzed for cell viability and cytoskeleton morphology.

Quantifying cell viability/proliferation and matrix organization

To determine if viability/proliferation is affected by cyclic stretching, nuclei were stained after both static and stretch protocols (Figure 3.1A(i-ii)). As the cells were seeded at $2.0x10^5$ cells/well for all conditions, the final density quantified from the nuclei stain is a measure of the combined viability and proliferation potential. Compared to both Patients and Negative Controls, the Positive Control generally exhibited a lower cell density (Figure 3.1A(iii)). However, cyclically stretching the cells did not induce a change in viability/proliferation in either Patient or Positive Control groups. Interestingly, Patients cells also did not have a compromised cell viability/proliferation compared to the Negative Controls (Figure 3.1A(iii)). To quantify the effects of the *LMNA* mutation on the cytoskeleton and the extracellular matrix, orientation order parameter (OOP) was used as a measurement of organization for actin (Figure 3.1B) and fibronectin (Figure

3.1C) [19]. Without stretch, the tissues and underlying extracellular matrix remained isotropic (low OOP) with no differences observed in actin or fibronectin organization for all groups (Figure 3.1B(iii) & 3.1C(iii), purple bars). Conversely, cyclic stretching induced organization (high OOP) in both the tissues and the underlying fibronectin (Figure 3.1B(iii) & 3.1C(iii), yellow bars). Interestingly, in the Positive Control, actin and fibronectin were less organized post-stretch when compared to Negative Controls (Figure 3.1B(iii) & 3.1C(iii)). Yet, there were no differences observed in either actin or fibronectin organization between Patients and Negative Controls (Figure 3.1B(iii) & 3.1C(iii)).

Subtle effects of cyclic strain on nuclear morphology

To further assess if cells with *LMNA* mutations are vulnerable to cyclic strain, nuclear morphology was examined. Nuclei were automatically detected, categorized, and measured for morphological properties using custom software [16]. To determine if cells with the *LMNA* mutation are more vulnerable to deformities by cyclic strain, the percentage of defective nuclei was calculated in both static and stretch conditions (Figure 3.2A). The nuclei of Positive Control cells were found to be generally more defective than Patients and Negative Controls for both conditions (Figure 3.2B). However, no differences were found between Patients and Negative Controls in any of the conditions (Figure 3.2B). Interestingly, exposing cells to cyclic stretch did not increase the percentage of defective nuclei for any of the groups (Figure 3.2B).

For a more detailed analysis, the aspect ratio (Figure 3.2C) and area (Figure 3.2D) of the nuclei were measured. Aspect ratio, a measure of eccentricity, is one for perfectly circular nuclei (Figure 3.2C(iii), left) and less than one for elongated nuclei (Figure 3.2C(iii), right). Each variation of the *LMNA* mutation responded differently to cyclic strain (Figure 3.2C(i-ii)). The

nuclei of the Patients A group were more elongated compared to the Negative Controls in both static and stretch conditions (Figure 3.2C(i-ii)). In contrast, Patients C nuclei showed less elongation in general while Patient B nuclei showed no significant differences when compared to the Negative Controls (Figure 3.2C(i-ii)). As expected, Positive Control nuclei were the least elongated amongst all cell lines for both static and stretch conditions (Figure 3.2C(i-ii)) [16]. For nuclear area, cells with different *LMNA* mutations also exhibited varying responses (Figure 3.2D(i-ii)): Nuclei ranged from small (Figure 3.2D(iii), left) to large (Figure 3.2D(iii), right) areas for both static and stretch conditions. Though when summarized, Patients A and B groups did not show a change in nuclear area post-stretch while the Patients C group significantly increased in response to stretching (Figure 3.2D(i-ii)). In addition, the Patients B group showed no differences when compared to the Negative Controls in the static and stretch conditions, unlike both Patients A and C groups (Figure 3.2D(i-ii)). Similar to aspect ratio, Positive Control had the greatest nuclear area post-stretch compared to all Patient groups and Negative Controls (Figure 3.2D(i-ii)). When both area and aspect were compared by pooling individual patients instead of all patients and coverslips, many significances resulting from large sample sizes were removed. The Patients A group still had significantly more elongated nuclei when compared to the Patients C group and Negative Controls (Figure 3.2C(i), green lines). For area, only the Patients C group maintained a significant increase in nuclear area post-stretch (Figure 3.2D(i), green lines). Unlike all of the other cell-lines, upon exposure to cyclic stretching, the Patients C group exhibited a combination of nuclear area and aspect ratio changes indicating that either the nuclear volume increases or the height of the nuclei decreases in the Patients C group (Figure 3.6).

Consequences of exposure to extensive cyclic strain

The choice to expose fibroblasts to 24 hours of strain was dictated by experimental convenience, but it can be argued that one day or normal 15% strain is an insufficient amount of time and/or stretch to cause *LMNA* mutation driven changes. We therefore cultured matched Patient and Negative Control cell lines for 72 hours while exposing the cells to a higher strain. As a result of applying cyclic strain for 72 hours, Patient A1 cells (PA1), unlike Control A1 cells (CA1), showed decreased viability/proliferation (Figure 3.3B, yellow bars). Yet, neither CA1 nor PA1 showed increased amounts of defective nuclei as a result of longer exposure times to cyclic strain (Figure 3.3C). To further examine the effects of prolonged cyclic stretching, organization of tissues and underlying extracellular matrix were examined along with nuclear morphology (Figure 3.3D-G). Indeed, as observed in the 24-hour experiment, tissues remained isotropic with no differences in actin or fibronectin organization for all groups without stretching (Figure 3.3D & 3.3E, purple bars). Correspondingly, the presence of the 72-hour cyclic strain increased organization in actin and fibronectin for both CA1 and PA1 as it did for the 24-hour experiment (Figure 3.3D & 3.3E, yellow bars). For nuclear morphology, only subtle differences were observed among both individuals under all exposure conditions (Figure 3.3F & 3.3G). In addition, unlike CA1, exposure to cyclic strain did not induce an increase in nuclear area for PA1 from static to stretch conditions (Figure 3.3G, matching patterns of purple bars to yellow bars).

DISCUSSION

In this work, we examined if simplified myocardial-like strains are sufficient to induce a difference between cells with and without *LMNA* mutations. To achieve this, human fibroblast

lines were assessed for cytoskeleton and extracellular matrix organization, nuclear morphology, and viability after being exposed to uniaxial cyclic strain.

In analyzing the results, it is useful to note several differences between the dynamic mechanical environment inside the myocardium and on the planar silicon membranes. In the myocardium, with cells oriented in varying circumferential and longitudinal directions, at peak systole, a range of measured circumferential, radial, and longitudinal strains have been reported as -23 to -10%, 30 to 47%, -23 to 0% respectively [20-29]. In contrast, uniaxial strains, similar to *in vitro* models [30-32] and a significant simplification of the myocardial environment, were used to generated data for Figure 3.1-3.3. Additionally, there are known differences between cardiomyocytes and fibroblasts in their responses to strain; cardiomyocytes organize parallel to the direction of strain while fibroblasts organize orthogonally (Figure 3.5) [33-35]. Consequently, after the cells had organized (within two hours), stretching exposed fibroblasts to strains orthogonal to their cytoskeleton, which is different from the strains experienced by cells in the myocardium. Given that cyclic strain is suspected to be an important factor in *LMNA* mutation driven pathologies in the heart, these differences of how fibroblasts are exposed to strains should be considered when interpreting the results of these experiments.

The number of dysmorphic nuclei and viability/proliferation were first evaluated to see how strains similar to those within the myocardium affect cells with and without *LMNA* mutations. For our experiments, as the initial density was the same for all cell lines, the final density after each culturing period was used as a representative measure of viability/proliferation. If the results had shown significant differences between any of the experimental groups involving the Patients and Negative Controls, it would have been interesting to distinguish between viability and proliferation with either a live/dead viability assay or fluorescence activated cell sorting to assess

the number of apoptotic cells. However, as there were no significant differences in these experiments the groups, the measurement viability/proliferation is sufficient. Furthermore, the number of dysmorphic nuclei was defined as the number of irregularly shaped nuclei instead of nuclei with blebbing since the former more frequently leads to nuclear membrane rupturing and consequentially DNA damage [36]. From previous literature, both Lamin A/C knockout (*Lmna*$^{-/-}$) and lamin C-only expression (*Lmna*$^{LCO/LCO}$) mouse embryonic fibroblasts (MEFs) were found to have significantly higher amounts of irregular shaped nuclei compared to those with normal *LMNA* expression [12, 13, 36]. Similarly, our experiments using human fibroblasts with HGPS, one of the more severe variation of *LMNA* mutations, had significantly higher amounts of dysmorphic nuclei compared to Negative Controls (Figure 3.2B). Patients, known to have only one mutated *LMNA* allele [8-10], might be comparable to heterozygous Lamin A/C knockout (*Lmna*$^{+/-}$) MEFs [13]; both exhibited no significant increase in the number of dysmorphic nuclei when compared to their negative controls (Figure 3.2B and [13], respectively). For viability, Lammerding et al. quantified the number of apoptotic cells for MEFs with different *LMNA* mutations. Both *Lmna*$^{-/-}$ and *Lmna*$^{LCO/LCO}$ MEFs had similar viabilities compared to MEFs with normal *LMNA* expression, but when subjected to biaxial cyclic stretch, only the former had decreased viability [13]. In our experiments, HGPS had significantly lower cell viability compared to the Negative Controls in static conditions, but this was not exacerbated when cells were subjected to uniaxial cyclic stretching (Figure 3.1A(iii)). For both Patients and *Lmna*$^{+/-}$ MEFs, viability was not compromised or affected by cyclic stretching (Figure 3.1A(iii) and [13], respectively). The minor discrepancies seen in cell viability between our results and previous literature might be caused by not only the varying *LMNA* mutations in Patients, but also the differences between uniaxial and biaxial cyclic stretching. Although there is a disparity between external stretching, our

experiments, versus the strains applied to the nucleus within the cardiomyocytes, overall our results were mostly in line with what was expected from *LMNA* knockout mouse experiments [12, 13, 36].

To further examine *LMNA* mutations and their relation to heart diseases, nuclear morphology, cytoskeleton organization, and extracellular matrix organization were compared amongst the groups after exposure to cyclic stretching. As expected from previous literature [33-35], uniaxial cyclic stretching induced actin and fibronectin organization for all cell lines (Figure 3.1B(iii) & C(iii)). Predictably, since HGPS patients have severe skin abnormalities, HGPS cells had less organization post-stretch when compared to Negative Controls (Figure 3.1B(iii) & C(iii)). Interestingly, there were no differences in organization amongst Patients and Negative Controls for either static or stretch conditions (Figure 3.1B(iii) & C(iii)). When area and eccentricity were examined in previous literature, similar trends were observed where HGPS cells and *Lmna*$^{-/-}$ MEFs were rounder with nuclear areas comparable to their respective negative controls [12, 37, 38]. Indeed, for our experiments HGPS cells were also observed to be rounder and have similar sized nuclei when compared to Negative Controls (Figure 3.2C(i-ii) & D(i-ii)). For Patient groups, the inconsistencies seen amongst them may suggest that different mutations may have their own subtle and diverse effects on the mechanical properties of the nucleus as seen in Figure 3.6 [8-10].

The direct mechanisms of how the *LMNA* mutation affects cells and their nuclei are still largely unknown. However, it is possible that the mutation can have an effect on the cytoskeleton, and in turn, cellular morphology, which has been observed to influence nuclear shape and positioning [39, 40]. While the tissue characterization performed in our experiments does not provide direct measurements of cell morphology (Figure 3.2B), the lack of changes in actin organization in the three families compared to the negative controls suggests that cell morphology

is not likely to be the cause of the subtle differences found between the nuclear shapes in the three families (Figure 3.2C(i-ii) & D(i-ii), Figure 3.6). However, the possibility remains that there are subtle cell shape differences that could affect cell-lines with a mutation, which could be further investigated in the future with single cell experiments or by specifically staining for cell membrane proteins.

For each patient, it was also determined in a previous study that the amount of dysmorphic nuclei is negatively correlated to the age at which heart disease symptoms are first presented [16]. Thus, it was uncertain if subjecting these cell lines to cyclic stretching for just one day was adequate to induce disease-causing differences that take years to develop within these patients. Therefore, additional strain experiments were conducted on a patient cell line (PA1) with an early presentation age and the corresponding related control (CA1) to examine the effects of longer exposure times. When the percentage of defective nuclei was quantified, no significant changes were observed after prolonged exposure to cyclic strain for either CA1 or PA1 (Figure 3.3C). However, PA1 did exhibit a loss in viability/proliferation after 72 hours of higher magnitude cyclic stretching when compared to the 24-hour condition, but it only decreased to levels similar to CA1 (Figure 3.3B, hatch bars). While applying higher strains may induce a greater response, it is beyond the physiological strain ranges, 10 to 20% [30-32], and thus the scope of this manuscript. Altogether, increasing exposure time to cyclic stretching and the strain to peak intensities within the physiological range did not deviate our findings greatly from the shorter experiments and results of previous publications.

Regardless of exposure time, cyclic strain was found to be insufficient to consistently affect the number of defective nuclei, nuclear morphology, viability, and cytoskeleton and extracellular matrix organization. Unlike HGPS individuals, cells from Patients with primarily heart pathologies

just exhibited subtle differences in nuclear morphology, but they were not drastically different compared to cell lines with normal *LMNA* genotype. Thus, simple cyclic strains in fibroblasts within the physiological ranges of strain was insufficient to promote differences that would explain pathways leading to the main pathology of heart disease in these patients with *LMNA* mutations.

ACKNOWLEDGMENT

The authors would like to thank to the *LMNA* gene mutation families that participated in the study, Linda McCarthy for her help in culturing the cell lines, and Hamza Atcha for his help in verifying the strains of the silicone membranes. We would also like to thank Prof. Samuel Safran, Prof. Eran Bouchbinder, Ohad Cohen, and Dan Deviri for discussions related to the work.

FUNDING

This work was funded by the National Institutes of Health [NIH 1 R01 HL129008-01 (Grosberg, Zaragoza)]. The funders had no role in the study design, data collection, data analysis, interpretation of the data, writing of the manuscript, or decision for publication.

REFERENCES

1. Brayson, D. and C.M. Shanahan, *Current insights into LMNA cardiomyopathies: Existing models and missing LINCs.* Nucleus, 2017. **8**(1): p. 17-33.
2. Parnaik, V.K., *Role of nuclear lamins in nuclear organization, cellular signaling, and inherited diseases.* International Review of Cell and Molecular Biology, Vol 266, 2008. **266**: p. 157-206.
3. Gruenbaum, Y. and O. Medalia, *Lamins: the structure and protein complexes.* Current Opinion in Cell Biology, 2015. **32**: p. 7-12.
4. Shimi, T., et al., *Structural organization of nuclear lamins A, C, B1, and B2 revealed by superresolution microscopy.* Mol Biol Cell, 2015. **26**(22): p. 4075-86.
5. Andres, V. and J.M. Gonzalez, *Role of A-type lamins in signaling, transcription, and chromatin organization.* J Cell Biol, 2009. **187**(7): p. 945-57.
6. Gonzalez, J.M., et al., *Fast regulation of AP-1 activity through interaction of lamin A/C, ERK1/2, and c-Fos at the nuclear envelope.* Journal of Cell Biology, 2008. **183**(4): p. 653-666.
7. Zhong, N., et al., *Novel progerin-interactive partner proteins hnRNP E1, EGF, Mel 18, and UBC9 interact with lamin A/C.* Biochemical and Biophysical Research Communications, 2005. **338**(2): p. 855-861.
8. Zaragoza, M.V., et al., *Exome Sequencing Identifies a Novel LMNA Splice-Site Mutation and Multigenic Heterozygosity of Potential Modifiers in a Family with Sick Sinus Syndrome, Dilated Cardiomyopathy, and Sudden Cardiac Death.* PLoS One, 2016. **11**(5): p. e0155421.
9. Zaragoza, M.V., et al., *Heart-hand syndrome IV: a second family with LMNA-related cardiomyopathy and brachydactyly.* Clin Genet, 2017. **91**(3): p. 499-500.
10. Zaragoza, M.V., et al., *Dupuytren's and Ledderhose Diseases in a Family with LMNA-Related Cardiomyopathy and a Novel Variant in the ASTE1 Gene.* Cells, 2017. **6**(4).
11. Broers, J.L.V., et al., *Decreased mechanical stiffness in LMNA-/- cells is caused by defective nucleo-cytoskeletal integrity: implications for the development of laminopathies.* Human Molecular Genetics, 2004. **13**(21): p. 2567-2580.
12. Lammerding, J., et al., *Lamin A/C deficiency causes defective nuclear mechanics and mechanotransduction.* J Clin Invest, 2004. **113**(3): p. 370-8.
13. Lammerding, J., et al., *Lamins A and C but not lamin B1 regulate nuclear mechanics.* Journal of Biological Chemistry, 2006. **281**(35): p. 25768-25780.
14. Sullivan, T., et al., *Loss of A-type lamin expression compromises nuclear envelope integrity leading to muscular dystrophy.* Journal of Cell Biology, 1999. **147**(5): p. 913-919.
15. Zwerger, M., et al., *Myopathic lamin mutations impair nuclear stability in cells and tissue and disrupt nucleo-cytoskeletal coupling.* Human Molecular Genetics, 2013. **22**(12): p. 2335-2349.
16. Core, J.Q., et al., *Age of heart disease presentation and dysmorphic nuclei in patients with LMNA mutations.* PLoS One, 2017. **12**(11).
17. Stoppel, W.L., D.L. Kaplan, and L.D. Black, 3rd, *Electrical and mechanical stimulation of cardiac cells and tissue constructs.* Adv Drug Deliv Rev, 2016. **96**: p. 135-55.
18. Eriksson, M., et al., *Recurrent de novo point mutations in lamin A cause Hutchinson-Gilford progeria syndrome.* Nature, 2003. **423**(6937): p. 293-8.

19. Grosberg, A., et al., *Ensembles of engineered cardiac tissues for physiological and pharmacological study: Heart on a chip.* Lab on a Chip, 2011. **11**(24): p. 4165-4173.
20. Hurlburt, H.M., et al., *Direct ultrasound measurement of longitudinal, circumferential, and radial strain using 2-dimensional strain imaging in normal adults.* Echocardiography-a Journal of Cardiovascular Ultrasound and Allied Techniques, 2007. **24**(7): p. 723-731.
21. Ng, A.C.T., et al., *Findings from Left Ventricular Strain and Strain Rate Imaging in Asymptomatic Patients With Type 2 Diabetes Mellitus.* American Journal of Cardiology, 2009. **104**(10): p. 1398-1401.
22. Gjesdal, O., et al., *Global longitudinal strain measured by two-dimensional speckle tracking echocardiography is closely related to myocardial infarct size in chronic ischaemic heart disease.* Clinical Science, 2007. **113**(5-6): p. 287-296.
23. Kouzu, H., et al., *Left ventricular hypertrophy causes different changes in longitudinal, radial, and circumferential mechanics in patients with hypertension: a two-dimensional speckle tracking study.* J Am Soc Echocardiogr, 2011. **24**(2): p. 192-9.
24. Serri, K., et al., *Global and regional myocardial function quantification by two-dimensional strain: application in hypertrophic cardiomyopathy.* Journal of the American College of Cardiology, 2006. **47**(6): p. 1175-81.
25. Wang, J., et al., *Preserved left ventricular twist and circumferential deformation, but depressed longitudinal and radial deformation in patients with diastolic heart failure.* European Heart Journal, 2008. **29**(10): p. 1283-1289.
26. Waldman, L.K., Y.C. Fung, and J.W. Covell, *Transmural Myocardial Deformation in the Canine Left-Ventricle - Normal Invivo 3-Dimensional Finite Strains.* Circulation Research, 1985. **57**(1): p. 152-163.
27. Wang, J., et al., *Preserved left ventricular twist and circumferential deformation, but depressed longitudinal and radial deformation in patients with diastolic heart failure.* Eur Heart J, 2008. **29**(10): p. 1283-9.
28. Kasner, M., et al., *Global strain rate imaging for the estimation of diastolic function in HFNEF compared with pressure-volume loop analysis.* European Journal of Echocardiography, 2010. **11**(9): p. 743-751.
29. Leitman, M., et al., *Two-dimensional strain - A novel software for real-time quantitative echocardiographic assessment of myocardial function.* Journal of the American Society of Echocardiography, 2004. **17**(10): p. 1021-1029.
30. Nguyen, M.D., et al., *Effects of Physiologic Mechanical Stimulation on Embryonic Chick Cardiomyocytes Using a Microfluidic Cardiac Cell Culture Model.* Analytical Chemistry, 2015. **87**(4): p. 2107-2113.
31. Ghafar-Zadeh, E., J.R. Waldeisen, and L.P. Lee, *Engineered approaches to the stem cell microenvironment for cardiac tissue regeneration.* Lab on a Chip, 2011. **11**(18): p. 3031-3048.
32. Marsano, A., et al., *Beating heart on a chip: a novel microfluidic platform to generate functional 3D cardiac microtissues.* Lab on a Chip, 2016. **16**(3): p. 599-610.
33. Matsuda, T., et al., *N-cadherin-mediated cell adhesion determines the plasticity for cell alignment in response to mechanical stretch in cultured cardiomyocytes.* Biochem Biophys Res Commun, 2005. **326**(1): p. 228-32.
34. Salameh, A., et al., *Cyclic mechanical stretch induces cardiomyocyte orientation and polarization of the gap junction protein connexin43.* Circ Res, 2010. **106**(10): p. 1592-602.

35. Greiner, A.M., et al., *Cyclic tensile strain controls cell shape and directs actin stress fiber formation and focal adhesion alignment in spreading cells.* PLoS One, 2013. **8**(10): p. e77328.
36. Chen, N.Y., et al., *Fibroblasts lacking nuclear lamins do not have nuclear blebs or protrusions but nevertheless have frequent nuclear membrane ruptures.* Proc Natl Acad Sci U S A, 2018. **115**(40): p. 10100-10105.
37. Choi, S., et al., *Computational image analysis of nuclear morphology associated with various nuclear-specific aging disorders.* Nucleus, 2011. **2**(6): p. 570-579.
38. Booth-Gauthier, E.A., et al., *Hutchinson-Gilford progeria syndrome alters nuclear shape and reduces cell motility in three dimensional model substrates.* Integrative Biology, 2013. **5**(3): p. 569-577.
39. Lele, T.P., R.B. Dickinson, and G.G. Gundersen, *Mechanical principles of nuclear shaping and positioning.* J Cell Biol, 2018. **217**(10): p. 3330-3342.
40. Lee, H., et al., *Cytoskeletal prestress regulates nuclear shape and stiffness in cardiac myocytes.* Exp Biol Med (Maywood), 2015. **240**(11): p. 1543-54.

FIGURE CAPTION LIST

Figure 3.1 Consequences of cyclic strain on cell viability/proliferation and organization. (A) (i-ii) Example images of nuclei stained with DAPI (blue); (iii) Cell density estimated by nuclei count. (B) (i-ii) Example images of actin stained with Phalloidin (green); (iii) Quantification of actin organization. (C) (i-ii) Example images of samples stained for fibronectin (red); (iii) Quantification of extracellular matrix organization. (A-C) Scale bar: 25 μm; (i) Stains in the static condition; (ii) Stains in the stretch condition with black arrows indicating the direction of stretch; (iii) Connecting lines represent significances within conditions and between corresponding groups ($p<0.05$); Sample sizes listed within the bars. Summary of statistical analysis and sample sizes found in Table 3.1.

Figure 3.2 Consequences of cyclic strain on nuclear morphology. (A) Automatic nuclei detection, classification, and measurement of nuclear properties; nuclei are designated as defective (red) and normal (green) [16]. (B) Percent of defective nuclei; Sample size is the number of individual coverslips (#c.s.); Error bars represent the standard error of the mean; Connecting black lines represent significances between corresponding groups ($p<0.05$). (C-D) (i) Summary of aspect ratio (C) and area (D); Sample sizes: total nuclei number (n) and number of patients (#p); Error bars represent standard deviation calculated for nuclei by pooling all coverslips and patients (black) or individual patients (green); Green lines represent significances analyzed by individual patients ($p<0.05$); (ii) Significance matrix of (i) for individual nuclei, i.e., black error bars, with red numbers corresponding to the respective labeled group in plot; (iii) Example nuclei with a high aspect ratio or small area (left) and a low aspect ratio or large area (right). All scale bars: 25 μm. Summary of

statistical analysis and sample sizes found in Table 3.1. Data presented for separate individuals is plotted in Figure 3.4.

Figure 3.3 Exposure to extensive cyclic strain and its effects. (A) Summary of the three different cyclic stretching regimes/experiments; Insert scale bar: 25μm. (B) Cell density estimated by nuclei count. (C) Percent of defective nuclei; Error bars represent the standard error of the mean. (D) Quantification of actin organization. (E) Quantification of extracellular matrix organization. (F) Summary of aspect ratio for all nuclei in each experiment. (G) Summary of nuclear area for all nuclei in each experiment. (B-G) Static data shown in purple and stretched data in yellow; Patterns: solid bars for 24 hours of 15% cyclic strain and hatch bars for 72 hours of 20% cyclic strain; Significance matrixes of corresponding bars labeled in red (grey boxes $p<0.05$, white boxes $p>0.05$); Sample sizes denoted in white within bars. (B, D-G) Error bars represent the standard deviation. Summary of statistical analysis and sample sizes found in Table 3.2.

FIGURES

Figure 3.1:

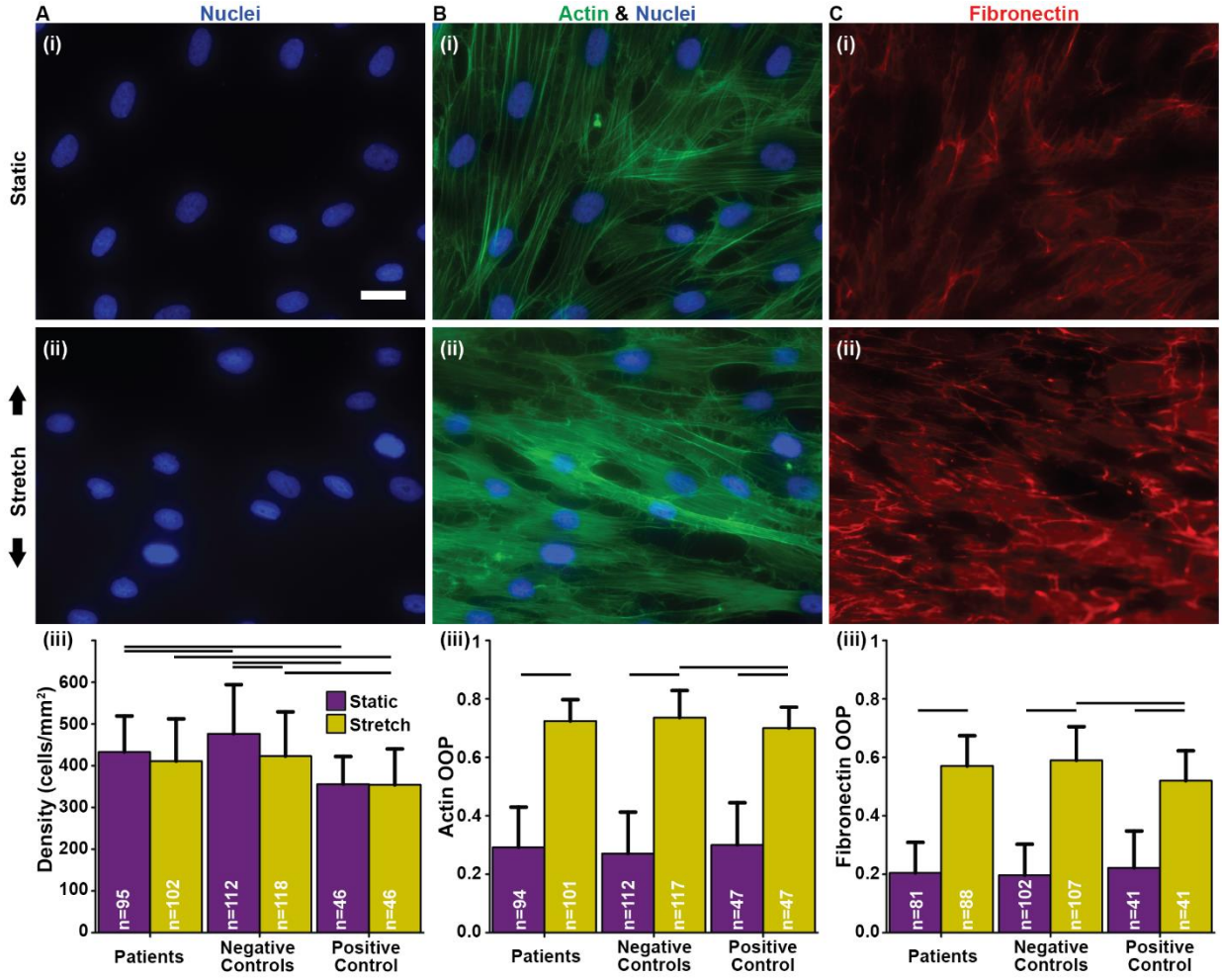

Figure 3.1 Consequences of cyclic strain on cell viability/proliferation and organization. (A) (i-ii) Example images of nuclei stained with DAPI (blue); (iii) Cell density estimated by nuclei count. (B) (i-ii) Example images of actin stained with Phalloidin (green); (iii) Quantification of actin organization. (C) (i-ii) Example images of samples stained for fibronectin (red); (iii) Quantification of extracellular matrix organization. (A-C) Scale bar: 25 μm; (i) Stains in the static condition; (ii) Stains in the stretch condition with black arrows indicating the direction of stretch; (iii) Connecting lines represent significances within conditions and between corresponding groups ($p<0.05$); Sample sizes listed within the bars. Summary of statistical analysis and sample sizes found in Table 3.1.

Figure 3.2:

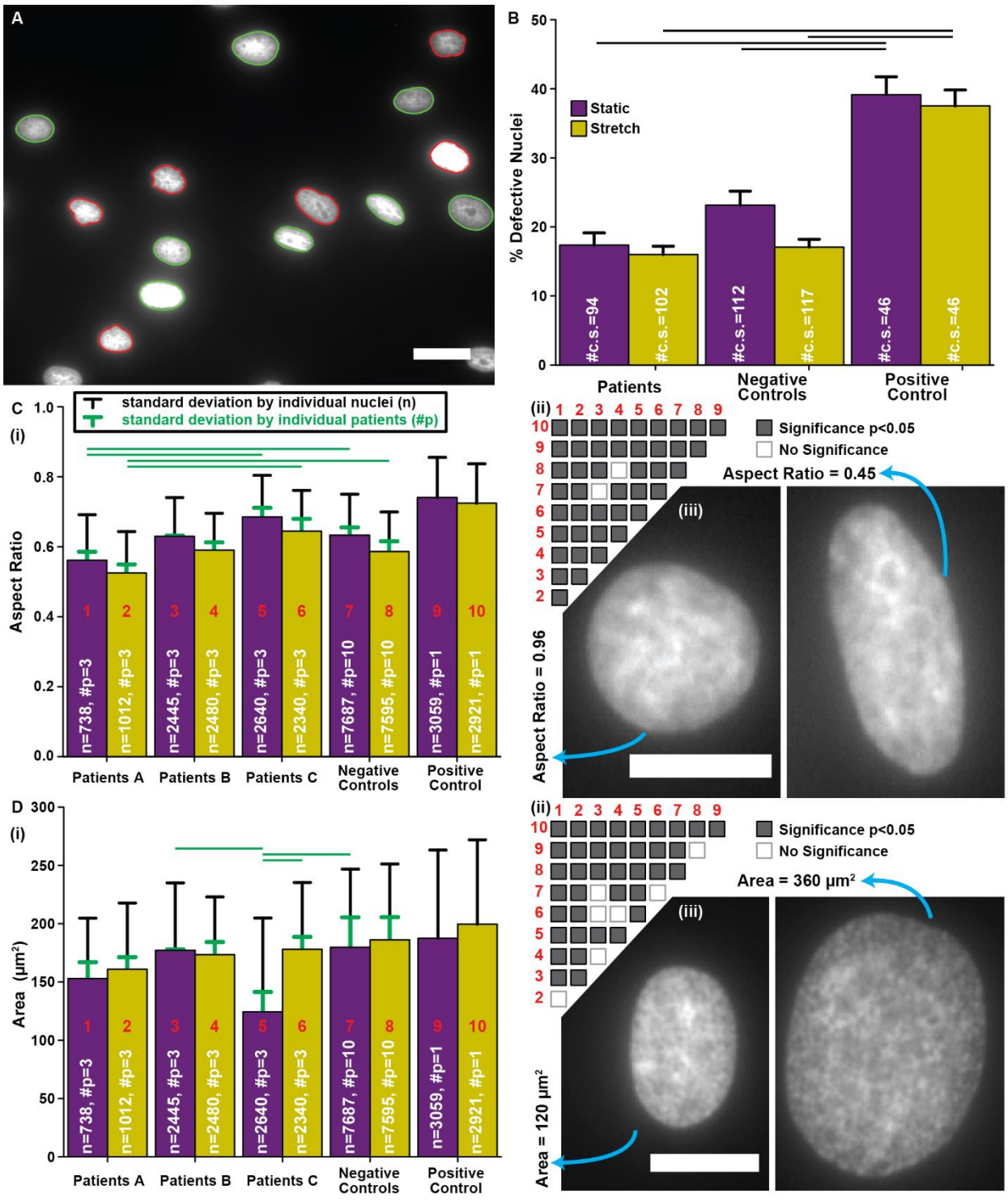

Figure 3.2 Consequences of cyclic strain on nuclear morphology. (A) Automatic nuclei detection, classification, and measurement of nuclear properties; nuclei are designated as defective

(red) and normal (green) [16]. (B) Percent of defective nuclei; Sample size is the number of individual coverslips (#c.s.); Error bars represent the standard error of the mean; Connecting black lines represent significances between corresponding groups ($p<0.05$). (C-D) (i) Summary of aspect ratio (C) and area (D); Sample sizes: total nuclei number (n) and number of patients (#p); Error bars represent standard deviation calculated for nuclei by pooling all coverslips and patients (black) or individual patients (green); Green lines represent significances analyzed by individual patients ($p<0.05$); (ii) Significance matrix of (i) for individual nuclei, i.e., black error bars, with red numbers corresponding to the respective labeled group in plot; (iii) Example nuclei with a high aspect ratio or small area (left) and a low aspect ratio or large area (right). All scale bars: 25 μm. Summary of statistical analysis and sample sizes found in Table 3.1. Data presented for separate individuals is plotted in Figure 3.4.

Figure 3.3:

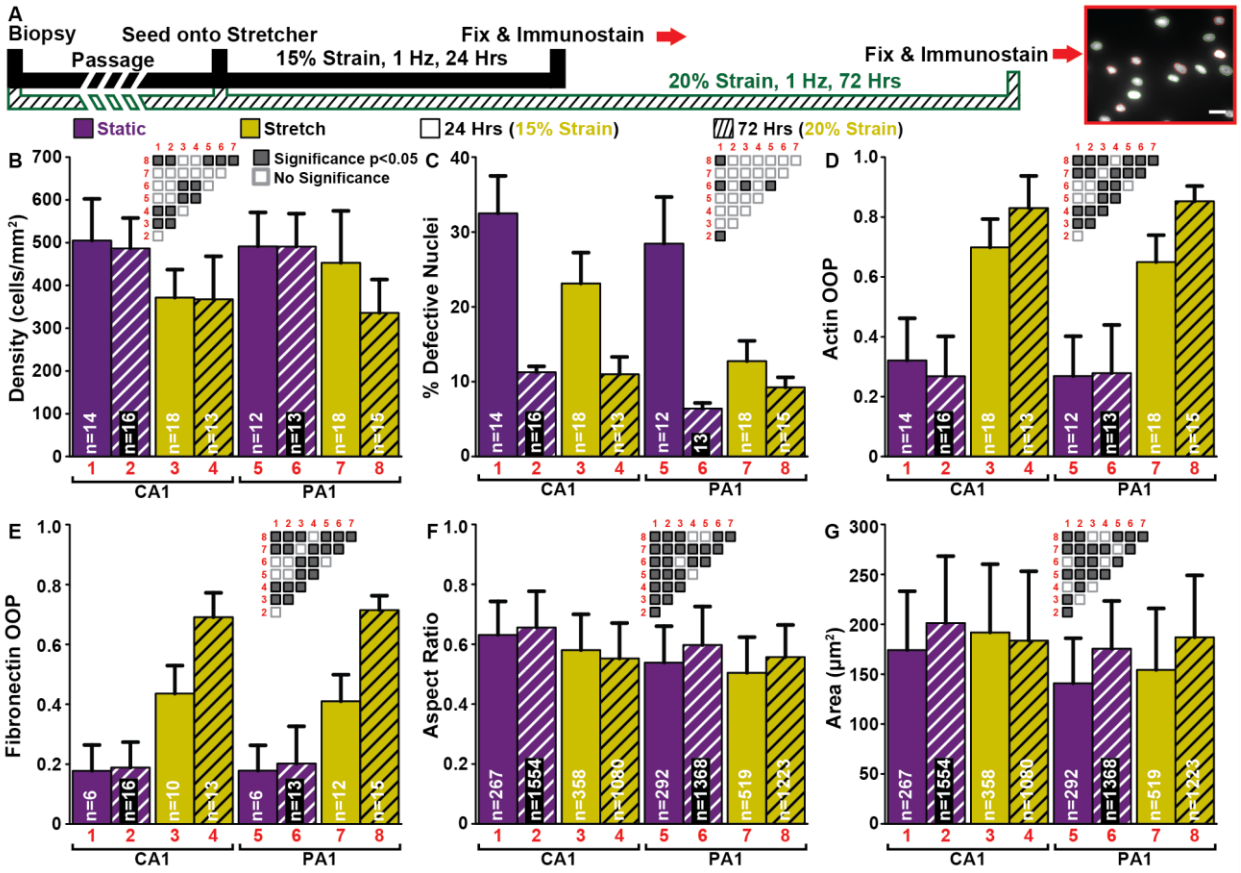

Figure 3.3 Exposure to extensive cyclic strain and its effects. (A) Summary of the three different cyclic stretching regimes/experiments; Insert scale bar: 25µm. (B) Cell density estimated by nuclei count. (C) Percent of defective nuclei; Error bars represent the standard error of the mean. (D) Quantification of actin organization. (E) Quantification of extracellular matrix organization. (F) Summary of aspect ratio for all nuclei in each experiment. (G) Summary of nuclear area for all nuclei in each experiment. (B-G) Static data shown in purple and stretched data in yellow; Patterns: solid bars for 24 hours of 15% cyclic strain and hatch bars for 72 hours of 20% cyclic strain; Significance matrixes of corresponding bars labeled in red (grey boxes $p<0.05$, white boxes $p>0.05$); Sample sizes denoted in white within bars. (B, D-G) Error bars represent the standard deviation. Summary of statistical analysis and sample sizes found in Table 3.2.

SUPPLEMENTARY FIGURE CAPTION LIST

Figure 3.4 Nuclear morphology of individual cell lines in response to cyclic stretching. (A) (i) Summary of aspect ratio for all nuclei in each group; (ii) Significance matrix with red numbers corresponding to the respective labeled group in plot. (B) (i) Summary of area for all nuclei in each group; (ii) Significance matrix with red numbers corresponding to the respective labeled group in plot.

Figure 3.5 Organizational directors of actin and fibronectin. (A) Quantification of both actin and extracellular matrix organizational directors of stretched cells; Stretch is along 0˚; No significances found (all $p>0.05$); Sample sizes denoted in within bars.

Figure 3.6 Cell height ratio of individual families. (A) The nuclei height ratio between the stretch and static conditions derived from area and aspect ratio (Figure 3.2C & 32D) for each family based on the assumption that nuclei, as ellipses, have constant volume. The inverse of this ratio represents the nuclei volume ratio between the stretch and static conditions when assuming constant nuclear height. Connecting lines represent significances within conditions and between corresponding groups ($p<0.05$); Sample sizes listed within the bars.

SUPPLEMENTAL FIGURES

Figure 3.4:

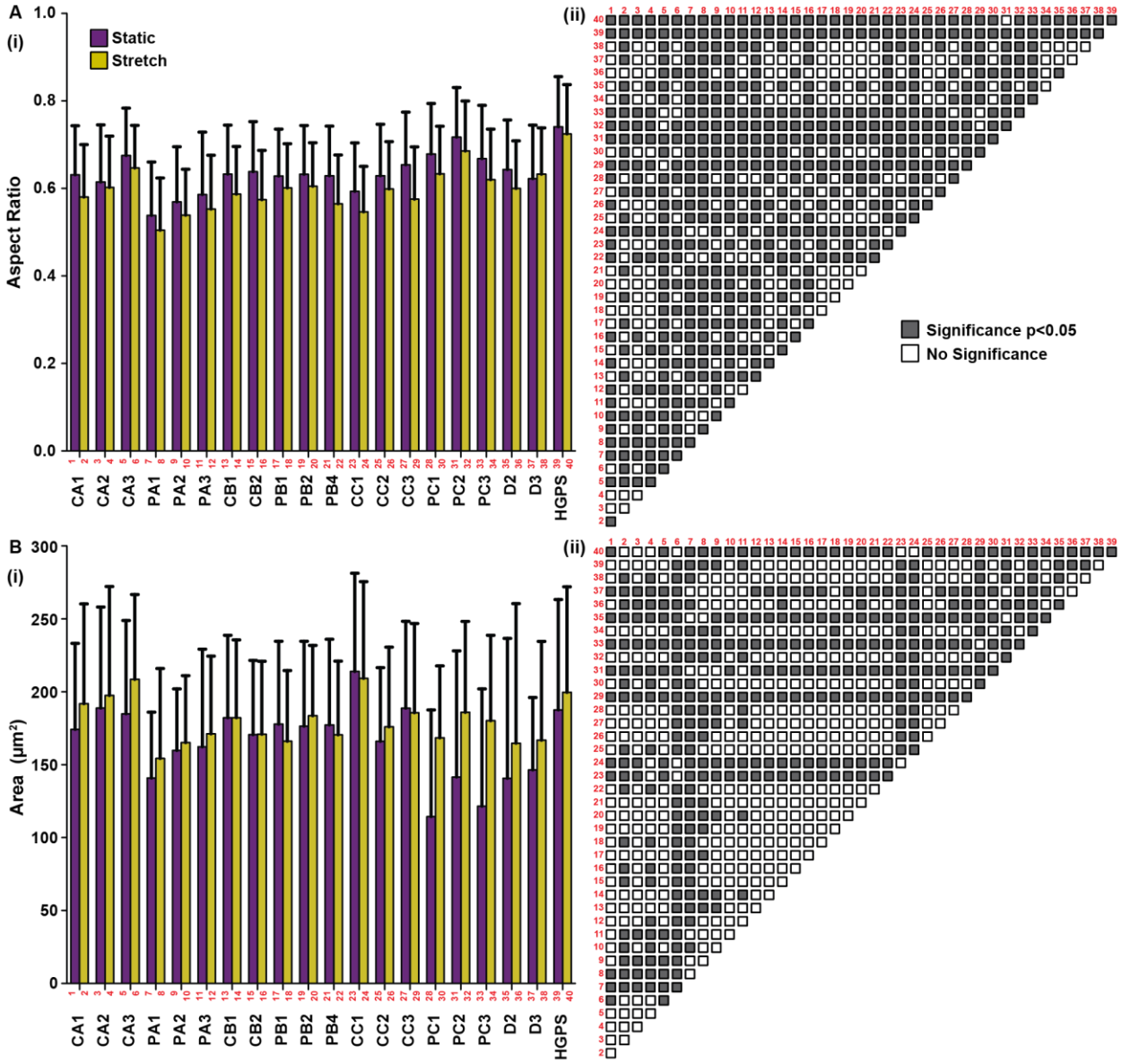

Figure 3.4 Nuclear morphology of individual cell lines in response to cyclic stretching. (A) (i) Summary of aspect ratio for all nuclei in each group; (ii) Significance matrix with red numbers corresponding to the respective labeled group in plot. (B) (i) Summary of area for all nuclei in each group; (ii) Significance matrix with red numbers corresponding to the respective labeled group in plot.

Figure 3.5:

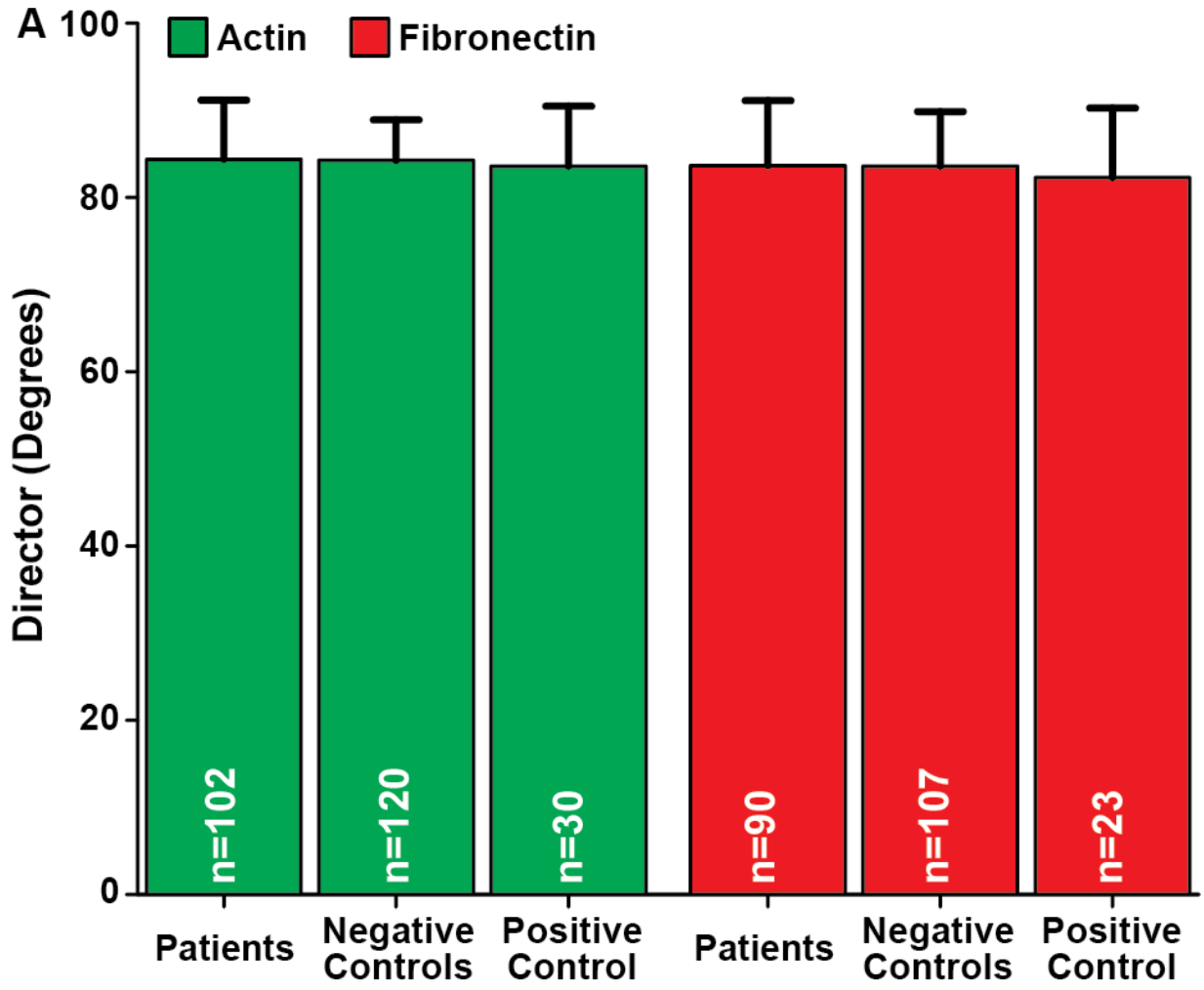

Figure 3.5 Organizational directors of actin and fibronectin. (A) Quantification of both actin and extracellular matrix organizational directors of stretched cells; Stretch is along 0˚; No significances found (all $p>0.05$); Sample sizes denoted in within bars.

Figure 3.6

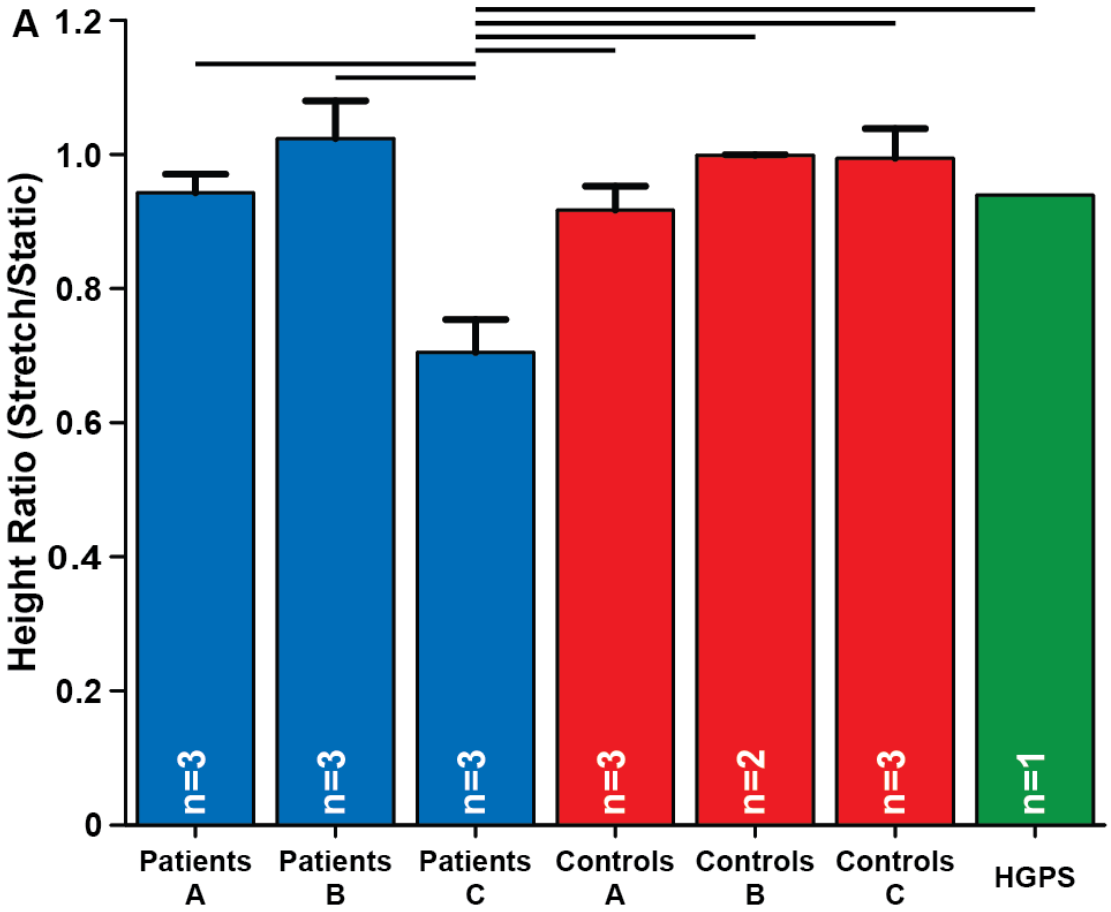

Figure 3.6 Nuclei height ratio of each family. (A) The nuclei height ratio between the stretch and static conditions derived from area and aspect ratio (Figure 3.2C & 3.2D) for each family based on the assumption that nuclei, as ellipses, have constant volume. The inverse of this ratio represents the nuclei volume ratio between the stretch and static conditions when assuming constant nuclear height. Connecting lines represent significances within conditions and between corresponding groups ($p<0.05$); Sample sizes listed within the bars.

TABLE CAPTION LIST

TABLES

Table 3.1 Summary of sample sizes of statistically tested groups.

I. Metric	II. Experimental Groups	III. Condition	IV. Compiled Number of Nuclei	V. Number of Coverslips	VI. Number of Individuals	VII. Test & Sample Size Used
Density	Patients	Static	14629	95	9	ANOVA Coverslips (Column V)
		Stretch	15065	102		
	Negative Controls	Static	17492	112	10	
		Stretch	16450	118		
	Positive Controls	Static	5789	46	1	
		Stretch	5751	46		
Actin OOP	Patients	Static	N/A	94	9	ANOVA Coverslips (Column V)
		Stretch		101		
	Negative Controls	Static	N/A	112	10	
		Stretch		117		
	Positive Controls	Static	N/A	47	1	
		Stretch		47		
Fibronectin OOP	Patients	Static	N/A	81	9	ANOVA Coverslips (Column V)
		Stretch		88		
	Negative Controls	Static	N/A	102	10	
		Stretch		107		
	Positive Controls	Static	N/A	41	1	
		Stretch		41		
% Defective Nuclei	Patients	Static	5823	94	9	Kruskal-Wallis & Dunn's Multiple Comparison Coverslips (Column V)
		Stretch	5832	102		
	Negative Controls	Static	7687	112	10	
		Stretch	7595	117		
	Positive Controls	Static	3059	46	1	
		Stretch	2921	46		
Aspect Ratio & Area	Patients A	Static	738	33	3	ANOVA Nuclei (Column IV) & Individuals (Column VI)
		Stretch	1012	40		
	Patients B	Static	2445	30	3	
		Stretch	2480	30		
	Patients C	Static	2640	31	3	
		Stretch	2340	32		
	Negative Controls	Static	7687	112	10	
		Stretch	7595	117		
	Positive Controls	Static	3059	46	1	
		Stretch	2921	46		

Table 3.2 Summary of sample sizes of statistically tested groups for 72-hour experiments.

I. Metric	II. Experimental Groups	III. Condition	IV. Compiled Number of Nuclei	V. Number of Coverslips	VI. Test & Sample Size Used
Density	Control A1	Static	2513	14	ANOVA Coverslips (Column V)
		Stretch	2390	18	
	Control A1 (72 Hours)	Static	2602	16	
		Stretch	1713	13	
	Patient A1	Static	2108	12	
		Stretch	2922	18	
	Patient A1 (72 hours)	Static	2293	13	
		Stretch	1839	15	
Actin OOP	Control A1	Static	N/A	14	ANOVA Coverslips (Column V)
		Stretch		18	
	Control A1 (72 Hours)	Static	N/A	16	
		Stretch		13	
	Patient A1	Static	N/A	12	
		Stretch		18	
	Patient A1 (72 hours)	Static	N/A	13	
		Stretch		15	
Fibronectin OOP	Control A1	Static	N/A	6	ANOVA Coverslips (Column V)
		Stretch		10	
	Control A1 (72 Hours)	Static	N/A	16	
		Stretch		13	
	Patient A1	Static	N/A	6	
		Stretch		12	
	Patient A1 (72 hours)	Static	N/A	13	
		Stretch		15	
% Defective Nuclei	Control A1	Static	267	14	Kruskal-Wallis & Dunn's Multiple Comparison Coverslips (Column V)
		Stretch	358	18	
	Control A1 (72 Hours)	Static	1554	16	
		Stretch	1080	13	
	Patient A1	Static	292	12	
		Stretch	519	18	
	Patient A1 (72 hours)	Static	1368	13	
		Stretch	1223	15	
Aspect Ratio & Area	Control A1	Static	267	14	ANOVA Nuclei (Column IV)
		Stretch	358	18	
	Control A1 (72 hours)	Static	1554	16	
		Stretch	1080	13	
	Patient A1	Static	292	12	
		Stretch	519	18	
	Patient A1 (72 hours)	Static	1368	13	
		Stretch	1223	15	

CHAPTER 4

CONCLUSION AND FUTURE WORKS

The heart can be vulnerable to a variety of diseases throughout a lifetime. However, due to the complexity of the heart, it is difficult to study these diseases and the possible treatment options. Thus, *in vitro* models are needed to recapitulate the heart in a simpler platform where it is possible to examine the cardiac mechanisms methodically and thoroughly. In this thesis, we addressed this necessity by utilizing a combination of engineering approaches to recapitulate the myocardial environment *in vitro* in order to facilitate the investigation of how healthy or pathological hearts develop or remodeled.

The heart has a unique mechanical environment that is contributed by its unique cells and structure. In Chapter 2, we combined the unique cellular composition and the dynamic mechanical environment of the heart into an *in vitro* experimental platform in order to understand vital cardiac processes such as cardiac remodeling and repair. The results indicated that cardiomyocytes and fibroblasts, two of the most abundant cell types in the heart, can influence the organization of one another in co-cultures depending on the seeding densities[1,2]. Additionally, we were able to replicate the organization found in healthy tissue and fibrotic heart tissue with these densities. Furthermore, we examined if intercellular junctions that mechanically and electrically couple cells to one another were potentially a factor that could play an influential role in controlling fibroblast and cardiomyocyte alignment in the heart[1,3–9]. However, when we inhibited these junctions in all of the co-cultures of densities, there were no differences in the organization when compared to controls. This suggests that these junctions do not play a dominant role in influencing the organization of tissue in our experiments. Overall, from this work, we contributed to the

understand of how cells organize in the heart while providing working densities to create *in vitro* models of healthy or fibrotic heart tissue.

Though our experiments successfully captured and replicated the organization found in healthy and fibrotic heart tissue, there are several differences between our cultures and the myocardial environment *in vivo*. The density at which organization resembling that of healthy heart tissue in our experiments occurred when cardiomyocytes occupied approximately 80% of the culture. In contrast, in the ventricles of the heart, there is twice the amount of cardiomyocytes when compared to fibroblasts[10-12]. One of the possible reasons that can explain the differences observed is that the heart has a laminar hierarchy, which consists of layers or "sheets" of muscle a few myocytes thick connected by collagen fibers[13–15]. In result, cells in the heart are surrounded by extracellular matrix proteins and others cells in all directions, increasing both extracellular matrix and cell-cell contact, respectively. Though our monolayer cultures are representative of a single sheet within the laminar hierarchy, the difference in amount of cell-cell or extracellular matrix contact could potentially explain the shift in the organization of the healthy tissue *in vitro* versus *in vivo*. The difference in structure could also explain why inhibition of junctions did not have an effect on the tissue organization. Hence, future models and work originating from this study should investigate the topic of organization in a 3D environment where cells can have more contact and communication. With a 3D experimental platform that incorporates both the dynamic mechanical environment of the heart and its unique cellular composition, it would be interesting to see how cardiomyocytes and fibroblasts behave in the new environment.

In Chapter 3, we continued utilizing the dynamic mechanical environment of the heart to study its effects on patient cells with genetic mutations that generally lead to heart diseases. We exposed these patients' skin fibroblasts to uniaxial cyclic strain and then quantified the cell

viability/proliferation, cytoskeleton and extracellular matrix organization, proportion of dysmorphic nuclei, and nuclear shape. We were able to observe some subtle differences in the nuclear shape in cells with *LMNA* mutations compared to those without. However, there were no significant differences in the viability, organization, or number of defective nuclei. As observed in Chapter 2, cardiomyocytes and fibroblasts responded to mechanical strain differently with each cell type organizing either approximately parallel or perpendicular to the strain direction, respectively. Thus, the strains experienced by the nuclei of skin fibroblasts and cardiomyocytes are intrinsically different. This may explain why we were unable to discern any significant differences in the skin fibroblasts of these patients with the *LMNA* mutation after exposure to cyclic strain.

To further investigate how the dynamic mechanical environment affects cells with genetic mutations, the next steps would entail using patient specific cardiac cells with the *LMNA* mutation. From our previous work in Chapter 2, we demonstrated that cardiomyocytes and fibroblasts respond differently to cyclic strain. Thus, patient specific cardiomyocytes may respond to cyclic strain differently and could potential elucidate the mechanisms leading to heart disease in cells with the *LMNA* mutation. However, cardiac cells remain inaccessible and cannot be taken from a patient. Thus, stem cells or an alternative cell source is needed to continue this study. In search of a possible solution, we found that cells shed in urine could be cultured, reprogrammed into stem cells, and then differentiated into cardiomyocytes[16–19]. Additionally, cells sourced from urine are easily accessible and the method is much less invasive than skin biopsies. With these cells, the investigation into how cyclic strain affects cells with the *LMNA* mutation can continue while also conducting functional and structural studies of engineered cardiac tissue with this mutation. Future

work with urine cells will expand the scope of these studies to include other genetic mutations and a larger population.

The results of this thesis demonstrates the importance of the dynamic mechanical environment of the heart as well as its cellular composition in studying heart development and diseases. We present a unique method of using engineering techniques to recapitulate the myocardial environment *in vitro* in order to study cardiac remodeling, repair and disease progression. The work done in this thesis advances our understanding of the heart and how it develops with and without diseases.

REFERENCES

1. Meghan B Knight, Anna Grosberg, and Megan L McCain. In Vitro Tools for Quantifying Structure–Function Relationships in Cardiac Myocyte Cells and Tissues. In *Cardiac Cytoarchitecture*, pages 15–39. Springer, 2015.
2. H. W. Vliegen, A. Van Der Laarse, C. J. Cornelisse, and F. Eulderink. Myocardial changes in pressure overload-induced left ventricular hypertrophy: A study on tissue composition, polyploidization and multinucleation. *European Heart Journal*, 12(4):488–494, 1991. ISSN 0195668X. doi: 10.1093/oxfordjournals.eurheartj.a059928.
3. A Salameh, A Wustmann, S Karl, K Blanke, D Apel, D Rojas-Gomez, H Franke, F W Mohr, J Janousek, and S Dhein. Cyclic mechanical stretch induces cardiomyocyte orientation and polarization of the gap junction protein connexin43. *Circulation Research*, 106(10):1592–1602, 2010. ISSN 1524-4571 (Electronic) 0009-7330 (Linking). doi: 10.1161/CIRCRESAHA.109.214429. URL http://www.ncbi.nlm.nih.gov/pubmed/20378856.
4. Carolina Vasquez, Poornima Mohandas, Karen L. Louie, Najate Benamer, Ashwini C. Bapat, and Gregory E. Morley. Enhanced fibroblast-myocyte interactions in response to cardiac injury. *Circulation Research*, 107(8), 2010. ISSN 00097330. doi: 10.1161/CIRCRESAHA.110.227421.
5. Patrizia Camelliti, Thomas K. Borg, and Peter Kohl. Structural and functional characterisation of cardiac fibroblasts, 2005. ISSN 00086363.
6. Thomas Desplantez, Emmanuel Dupont, Nicholas J. Severs, and Robert Weingart. Gap junction channels and cardiac impulse propagation, 2007. ISSN 00222631.
7. Yang Li, Chelsea D. Merkel, Xuemei Zeng, Jonathon A. Heier, Pamela S. Cantrell, Mai Sun, Donna B. Stolz, Simon C. Watkins, Nathan A. Yates, and Adam V. Kwiatkowski. The N-cadherin interactome in primary cardiomyocytes as defined using quantitative proximity proteomics. *Journal of cell science*, 132 (3), 2019. ISSN 14779137. doi: 10.1242/jcs.221606.
8. P. Zhang, J. Su, and U. Mende. Cross talk between cardiac myocytes and fibroblasts: From multiscale investigative approaches to mechanisms and functional consequences. *American Journal of Physiology - Heart and Circulatory Physiology*, 303(12), 2012. ISSN 03636135. doi: 10.1152/ajpheart.01167.2011.
9. Jiahn Chun Wu, Ru Yin Tsai, and Tun Hui Chung. Role of catenins in the development of gap junctions in rat cardiomyocytes. *Journal of Cellular Biochemistry*, 88(4):823–835, 2003. ISSN 07302312. doi: 10.1002/jcb.10390.
10. Richard A. Lasher, Aric Q. Pahnke, Jeffrey M. Johnson, Frank B. Sachse, and Robert W. Hitchcock. Electrical stimulation directs engineered cardiac tissue to an age-matched native phenotype. *Journal of Tissue Engineering*, 3(1), 2012. ISSN 20417314. doi: 10.1177/2041731412455354.
11. Peter Kohl and Robert G. Gourdie. Fibroblast-myocyte electrotonic coupling: Does it occur in native cardiac tissue?, 2014. ISSN 10958584.
12. Ana Rita M.P. Santos, Yongjun Jang, Inwoo Son, Jongseong Kim, and Yongdoo Park. Recapitulating cardiac structure and function in vitro from simple to complex engineering, 2021. ISSN 2072666X.

13. I. J. LeGrice, B. H. Smaill, L. Z. Chai, S. G. Edgar, J. B. Gavin, and P. J. Hunter. Laminar structure of the heart: Ventricular myocyte arrangement and connective tissue architecture in the dog. *American Journal of Physiology - Heart and Circulatory Physiology*, 269(2 38-2), 1995. ISSN 03636135. doi: 10.1152/ajpheart.1995.269.2.h571.
14. I. J. LeGrice, P. J. Hunter, and B. H. Smaill. Laminar structure of the heart: A mathematical model. *American Journal of Physiology - Heart and Circulatory Physiology*, 272(5 41-5), 1997. ISSN 03636135. doi: 10.1152/ajpheart.1997.272.5.h2466.
15. T. F. Robinson, M. A. Geraci, E. H. Sonnenblick, and S. M. Factor. Coiled perimysial fibers of papillary muscle in rat heart: Morphology, distribution, and changes in configuration. *Circulation Research*, 63 (3), 1988. ISSN 00097330. doi: 10.1161/01.RES.63.3.577.
16. Ting Zhou, Christina Benda, Sarah Dunzinger, Yinghua Huang, Jenny Cy Ho, Jiayin Yang, Yu Wang, Ya Zhang, Qiang Zhuang, Yanhua Li, Xichen Bao, Hung Fat Tse, Johannes Grillari, Regina Grillari Voglauer, Duanqing Pei, and Miguel A. Esteban. Generation of human induced pluripotent stem cells from urine samples. *Nature Protocols*, 7(12), 2012. ISSN 17502799. doi: 10.1038/nprot.2012.115.
17. Yuanyuan Zhang, Elena McNeill, Hong Tian, Shay Soker, Karl Erik Andersson, James J. Yoo, and Anthony Atala. Urine Derived Cells are a Potential Source for Urological Tissue Reconstruction. *Journal of Urology*, 180(5), 2008. ISSN 00225347. doi: 10.1016/j.juro.2008.07.023.
18. Lihui Wang, Linli Wang, Wenhao Huang, Huanxing Su, Yanting Xue, Zhenghui Su, Baojian Liao, Haitao Wang, Xichen Bao, Dajiang Qin, Jufang He, Wutian Wu, Kwok Fai So, Guangjin Pan, and Duanqing Pei. Generation of integration-free neural progenitor cells from cells in human urine. *Nature Methods*, 10(1), 2013. ISSN 15487091. doi: 10.1038/nmeth.2283.
19. Angelika Dörrenhaus, Jill I.F. Müller, Klaus Golka, Peter Jedrusik, Harald Schulze, and Wolfram Föllmann. Cultures of exfoliated epithelial cells from different locations of the human urinary tract and the renal tubular system. *Archives of Toxicology*, 74(10), 2000. ISSN 03405761. doi: 10.1007/s002040000173.

.

APPENDIX

CellScale MechanoCulture FX-2 Stretcher Protocol

Written by: Richard Tran & Ali Hatem Salaheldin Hassan Ahmed Hetta

Created by: Richard Tran

Day 1: Passaging Fibroblasts

NOTE: Passaging must be done at least once after initial preplate to get fibroblast to normal confluent morphology. Fibroblast should be left alone for at least two days before the experiments to recover and reach confluency.

Materials and Preparation for flasks **only**:

- ✓ Complete Media warmed in 37°C water bath
- ✓ Wash Solution (HBSS –ions, PBS –ions) warmed in water bath at 37°C
- ✓ Trypsin warmed in water bath at 37°C
- ✓ Trypsin Neutralizing Solution (Complete Media, TNS) warmed in water bath at 37°C
- ✓ Conicals, serological, pipette tips, Pasteur pipettes
- ✓ PBS warmed in 37°C water bath

1. Under the microscope, check TC flask for confluency. Passage when cells are 70-90% confluent if contact inhibited.
2. Aspirate media.
3. Add appropriate amount of wash solution (HBSS or PBS) and gently rock TC flask.
4. Aspirate wash solution.
5. Perform second wash by repeating steps 3 and 4.

6. Perform third wash by repeating steps 3 and 4.
7. Add appropriate amount of Trypsin to TC flask and place in incubator for 2 minutes.
8. Remove TC flask from incubator and check under microscope for detached cells. If cells are not rounded and free floating in suspension, gently tap TC flask and/or place back in incubator for additional 1-2 minutes. Use microscope to check cell detachment.
9. Add appropriate amount of Trypsin Neutralizing Solution (Media) to flask.
10. Transfer cell suspension from TC flask into conical.
11. Wash TC flask with Trypsin Neutralizing Solution and add suspension to conical.
12. Centrifuge conical at 1000 rpm for 5 minutes.
13. Aspirate supernatant leaving cell pellet untouched.
14. Resuspend cell pellet in complete media (1 -4 ml based on size of cell pellet).
15. Carefully break up cell pellet by gently pipetting with 1000 μL pipettor.
16. Add to flask with media and return to the incubator.

Day 2: Well Preparation

Materials needed for well preparation:

- ✓ autoclave pouch
- ✓ 150mm petri dishes
- ✓ 1mL micropipette
- ✓ 1mL micropipette tips
- ✓ PBS
- ✓ Sterile H2O
- ✓ Human fibronectin
- ✓ Parafilm

- ✓ Pasteur pipette
- ✓ 10mL serologicals
- ✓ Stretcher device and tools & 16 well plates (0.20 mm thickness)

Autoclave well plates

1. Place the well plates in an autoclave pouch and seal.
2. Once sealed, place the autoclave pouch in the autoclave machine and press “cycle select”, then “Dry 20”, and finally press “start”.
3. Leave the autoclave machine to run for approximately 1hr.

Preparing Diluted Fibronectin Solution

1. Spray necessary materials into the hood.
2. Make appropriate amount of 1:10 human fibronectin solution by adding 1080 µL of sterile water to 120 µL of aliquoted human fibronectin (Add slowly to the walls of the vial).
3. Leave the fibronectin to dissolve in the sterile water for approximately 8 mins.
4. During the 8 mins spray in all parts of the stretcher device and assemble. Attach autoclaved well plate to the device.
5. After assembling, ensure that the wells are stretched and left at maximum stretch position before proceeding to the next steps.

Cleanup

1. Pipette tips and serological tubes should be disposed of in biohazard waste container.

Adding fibronectin to wells

NOTE: When sealing the stretcher with parafilm make sure to slide the parafilm between the actuator and wells.

1. Wash the wells with PBS by filling them up halfway using a 10mL serological.
2. Once PBS is added to each all the wells cover stretcher wells with lid, and rock the stretcher gently.
3. Aspirate PBS using the Pasteur pipette.
4. Repeat steps 2 and 3 twice more to fully wash the wells.
5. Using a 1mL micropipette, add 150 µL of the fibronectin solution to each well.
6. Place the stretcher lid over the well.
7. Make sure the well bottom is fully covered with fibronectin. If not, gently tap on the sides of the stretcher device to spread the fibronectin.
8. Spray in parafilm and wrap the stretcher at the seam to ensure a tight seal.
9. Place the stretcher in a 4°C fridge overnight (~12 hr).

Cleanup

1. Tips, serologicals, and conicals should be disposed of in biohazard waste container.
2. Pasteur pipette should be disposed of in sharps biohazard waste container.

Day 3: Seeding Stretcher

Materials needed for seeding stretcher:

- ✓ 10mL serologicals
- ✓ Pasteur pipette
- ✓ PBS
- ✓ Trypsin
- ✓ Media
- ✓ 15mL conical tubes
- ✓ 1mL, 200 µL, and 10 µL micropipette tips

- ✓ C-chips
- ✓ Trypan blue

1. Spray in materials into the hood.
2. Prepare necessary cell solution. *Refer to* ***Passaging***.
3. Aspirate the fibronectin using a Pasteur pipette.
4. Gently wash wells 1-3 times with PBS to remove excess fibronectin using a 10mL serological.
5. Fill up wells with prepared cells, making sure to rock the wells in order to evenly spread the cells (maximum volume for each well 300 μL).
6. Place stretcher device in a 37°C incubator and start the actuator with a set program.

Cleanup

1. Serologicals and conicals should be disposed of in biohazard waste container.
2. Pasteur pipette should be disposed of in sharps biohazard waste container.

Day 4: Changing media

Materials needed for changing media:

- ✓ 10mL serologicals
- ✓ Media
- ✓ Pasteur pipettes
- ✓ PBS
- ✓ 1mL micropipette tips

Wash wells and add new media

NOTE: This procedure explains how to wash cells once, however, it is recommended that cells be washed 3 times. If cells are sensitive wash 1-2 times.

1. Spray in materials and stretcher.
2. Aspirate the media using a Pasteur pipette.
3. Wash wells with PBS using a 10mL serological. Add gently to not disturb cells.
4. Once PBS is added to each well cover stretcher wells with lid, and rock the stretcher gently.
5. Aspirate using the Pasteur pipette at a corner until there is little to no PBS left in the wells.
6. Repeat steps 2-5, two more times.
7. Fill up wells with media using a 1mL micropipette.
8. Return stretcher device to the incubator and start the actuator again if necessary.

Cleanup

1. Serologicals and conicals should be disposed of in biohazard waste container.
2. Pasteur pipette should be disposed of in sharps biohazard waste container.

Day 5: Fixing and Immunostaining

NOTE: Stain should be protected from light

Materials needed in chemical hood:

- ✓ 16% PFA (found in flammable cabinet under chemical hood) (VWR #100503-916, Electron Microscopy Sciences #15710)
- ✓ Non-sterile PBS (Life Technologies #10010-049)
- ✓ Pipette-man
- ✓ (1) 25 mL serological
- ✓ Sharps chemical waste container (Found in cabinet below and to the left of the chemical hood)

- ✓ (1) Opaque 50 mL or greater glass bottle (clear glass bottle can be wrapped with aluminum foil if opaque bottle is not available).
- ✓ 10mL serologicals
- ✓ 16 wells of seeded and stretched cells inside stretcher device.
- ✓ Tweezers
- ✓ Small hole puncher
- ✓ rectangle glass slide

Preparing 4% PFA Solution

Important Safety Precautions:

- ☠ **PFA is extremely hazardous and should only be handled by a lab member who has been trained on the hazards and proper precautions to take when handling PFA**
- ☠ Do all PFA work with gloves, lab coat, and eye protection in the chemical hood
- ☠ All materials that come into contact with PFA are toxic and are NOT to be rinsed or disposed of in either the biological or regular waste
- ☠ Sharps chemical waste container should only be opened **inside** of the chemical hood

1. Label opaque glass bottle with the following:
   - ✓ 4% PFA
   - ✓ Date (must be changed monthly)
   - ✓ TOXIC
2. Pipette 30 mL of non-sterile PBS to opaque glass bottle.

3. Transfer 10 mL of the 16% PFA into the opaque glass bottle. The final diluted stock will produce 40 mL of 4% PFA.
4. Secure cap to bottle before cleaning hood. Final diluted stock should be protected from light at all times.

Cleanup

1. Serologicals used with **PBS** can be disposed of in normal waste outside of hood.
2. Serologicals used with **PFA** must be disposed of in **solid** chemical waste (in hood). If container is full, contact EH&S immediately to have waste container picked up and new waste container delivered.
3. Plastic transfer pipette must be disposed of in **solids** chemical waste container (in hood). If container is full, contact EH&S immediately to have waste container picked up and new waste container delivered.

Mixing Triton-X and PFA

1. Label foil-wrapped centrifuge tube with the following:

   Name & Date (On centrifuge tube, not foil)

   4% PFA + Triton-X (On centrifuge tube & lid)

   TOXIC (On centrifuge tube & lid and foil)
2. For each well that you intend to fix, add 150 µL of 4% PFA stock solution to 15mL centrifuge tube.
3. For each 2mL of PFA that you have isolated, add 1µL of Triton-X 100 (TX-100). TX-100 is a very viscous solution, so be sure not to submerge pipette-man past pipette tip when pipetting from TX-100 vile. When adding TX-100 to centrifuge tube, slowly move

pipette tip back and forth while pipetting the TX-100 into the 4% PFA solution. A string-like gel should be visible when pipetting the TX-100 into the PFA solution.

4. Seal the conical tube and place it in a water bath for approximately 5 mins.

Cleanup

1. Pipette tips and serological tubes should be disposed of in biohazard waste container.

Fixing Cells

1. Aspirate the media from the wells of the stretcher by placing the Pasteur pipette near the bottom corner of each well.
2. Wash wells with PBS using a 10mL serological.
3. Once PBS is added to each well cover stretcher wells with lid, and rock the stretcher gently.
4. Aspirate using the Pasteur pipette until there is no PBS left in any of the wells.
5. Repeat steps 1-4, two more times.
6. Into each well of the stretcher add 150 µL of the PFA/triton-X solution using the 200 µL micropipette.
7. After adding PFA/triton-X solution cover the stretcher wells with a lid and leave the stretcher for 10 mins to fix.
8. Aspirate the PFA/triton-X from the wells of the stretcher by placing the Pasteur pipette on the corner of each well.
9. Wash wells with PBS using a 10mL serological.
10. Once PBS is added to each well cover stretcher wells with lid, and rock the stretcher gently, make sure PBS is spread out.
11. Leave the PBS in the stretcher wells.

12. Aspirate the wells using the Pasteur pipette until there is no PBS left in any of the wells.
13. Repeat steps 8-11, two more times.

Cleanup

1. Pipette tips, Serologicals, and conicals should be disposed of in biohazard waste container. Anything sharp must be placed in sharp waste container (e.g. Pasteur pipette).

Separate Wells from Stretcher

NOTE: The techniques mentioned for separating the wells from the stretcher device are one of many, but this is the most recommended method of separation.

1. Remove the middle pin on the side holding together the base of the stretcher and the wells.
2. Then using the metal rod tool given with the stretcher begin to carefully create space between the metal pillars and wells by pushing down on the wells.
3. Once pillars have been separated from the wells remove the black frame surrounding the wells by unscrewing the two pins on opposite sides.
4. After wells have been completely separated place the wells on a petri dish until immunostaining.

Preparing Stains

NOTE: Make a bit more to ensure no lack of stain due to loss of volume to sides of vial. To ensure stain is properly spread, do so by taping the sides.

1. Prepare two 15mL conical tubes by wrapping them with aluminum foil and labeling one “primary” and the other “secondary”.
2. In both labeled conical tubes, for each well, prepare 150 µL of stain mixture in an eppendorf tube by mixing PBS and the appropriate amount of stain.

3. Vortex the primary conical tube for 5 seconds.
4. Repeat steps 2 and 3 for secondary stain.

Cleanup

1. Pipette tips, Serologicals, and conicals should be disposed of in biohazard waste container.

Primary Staining

1. Aspirate PBS from washes from the fixing.
2. Add 150 µL of the primary staining solution to each well.
3. After adding the primary stain leave the wells for approximately 1hr in a no light environment.

Cleanup

1. Serologicals and conicals should be disposed of in biohazard waste container.
2. Pasteur pipette should be disposed of in sharps biohazard waste container.

Wash wells

1. Aspirate the primary stain from the wells of the stretcher by placing the Pasteur pipette on the corner of each well.
2. Wash wells with PBS using a 10mL serological.
3. Once PBS is added to each well cover stretcher wells with lid, and rock the stretcher gently.
4. Repeat 2 times steps 1-3.

Cleanup

1. Serologicals and conicals should be disposed of in biohazard waste container.
2. Pasteur pipette should be disposed of in sharps biohazard waste container.

Secondary Staining

NOTE: To ensure stain is properly spread, do so by taping the sides.

1. Add 150 µL of the stain solution in the secondary conical tube, using a 1mL micropipette, into each well.
2. After adding the secondary stain leave the wells in a no light environment for approximately an hour.

Cleanup

1. Serologicals and conicals should be disposed of in biohazard waste container.
2. Pasteur pipette should be disposed of in sharps biohazard waste container.

Wash Wells

NOTE: This procedure explains how to wash cells once, however, it is recommended that cells be washed 1-3 times.

1. Aspirate the secondary stain from the wells of the stretcher by placing the Pasteur pipette on the corner of each well.
2. Wash wells with PBS using a 10mL serological.
3. Once PBS is added to each well cover stretcher wells with lid, and rock the stretcher gently.
4. Leave the PBS in the stretcher with the lid covering the wells for five minutes, in a no light environment.
5. After 5 seconds are complete aspirate using the Pasteur pipette until there is no PBS left in any of the wells.
6. Repeat steps 2-5 two more times.
7. Leave last wash in the wells.

Cleanup

1. Serologicals and conicals should be disposed of in biohazard waste container.
2. Pasteur pipette should be disposed of in sharps biohazard waste container.

Mounting wells on glass slides

NOTE: The general technique for hole punching wells is once the whole puncher is pressed in, apply pressure in a up to down motion then a left to right motion followed by a clockwise circle motion. Tweezers should be used to carefully remove the well from the hole puncher. Insert one end of the tweezer into the puncher and force a corner of the well down onto the cutting board.

2. Prepare one glass slide for each coverslip and label. If slide is dusty, blow clean with compressed air or clean with 70 % ethanol and dry.
3. Remove the well plate from the petri dish and place on a cutting board.
4. Aspirate the PBS before hole punching (four at a time to prevent drying).
5. Begin hole punching the wells using a small hole puncher.
6. Use the tweezers to remove the stamped well from the puncher and move them to the corresponding glass slides. Make sure to space them apart and keep the same orientation during transfer. Do not place the wells too close to the edges.
7. Once all the wells have been stamped, using the 1mL micropipette, place one drops of ProLong Gold over the wells.
8. Then place a drop of the ProLong Gold in between each well, to spread the ProLong Gold solution.
9. Once the ProLong Gold is added, place a micro coverslip glass over the wells covered with ProLong Gold. Let the ProLong Gold spread and gently tap to remove air bubbles.
10. Then use nail polish to seal the seams in between the glass slides.

11. Cover the glass slides in a no light penetrating container and leave it for at least 24hrs before imaging.
12. Once dry, slides can be used for imaging. If you are not imaging immediately, slides should be stored in a slide box or dark box in the -20˚ C freezer.

Cleanup

1. Serologicals and conicals should be disposed of in biohazard waste container.
2. Pasteur pipette should be disposed of in sharps biohazard waste container.